CORRELATION BASED VIRTUAL SOURCE IMAGING IN STRONGLY SCATTERING RANDOM MEDIA

JOSSELIN GARNIER* AND GEORGE PAPANICOLAOU†

Abstract. Array imaging in a strongly scattering medium is limited because coherent signals recorded at the array and coming from a reflector to be imaged are weak and dominated by incoherent signals coming from multiple scattering by the medium. If, however, an auxiliary passive array can be placed between the reflector to be imaged and the scattering medium then the cross correlations of the incoherent signals on this array can also be used to image the reflector. In this paper we show both in the weakly scattering paraxial regime and in strongly scattering layered media that this cross correlation approach produces images as if the medium between the sources and the passive array was homogeneous and the auxiliary passive array was an active one made of both sources and receivers.

Key words. Imaging, wave propagation, random media, cross correlation.

AMS subject classifications. 35R60, 86A15.

1. Introduction. Consider an array of sources and receivers that can be used to image a reflector whose location and reflectivity are not known. The sources are located at $(\vec{\boldsymbol{x}}_s)_{s=1}^{N_{\rm s}}$ and the receivers at $(\vec{\boldsymbol{x}}_r)_{r=1}^{N_{\rm r}}$, as in Figure 1.1 (the two arrays can be coincident). The array response matrix $(p(t,\vec{\boldsymbol{x}}_r;\vec{\boldsymbol{x}}_s))_{t\in\mathbb{R},r=1,\ldots,N_{\rm r},s=1,\ldots,N_{\rm s}}$ consists of the signals recorded by the rth receiver when the sth source emits a short pulse. We obtain an image by migrating the array response matrix to estimate the locations of reflectors in the medium. The Kirchhoff migration function [4, 5] at a search point $\vec{\boldsymbol{y}}^S$ is

$$\mathcal{I}(\vec{\boldsymbol{y}}^S)=\sum_{r=1}^{N_{\rm r}}\sum_{s=1}^{N_{\rm s}} p\big(\mathcal{T}(\vec{\boldsymbol{x}}_s,\vec{\boldsymbol{y}}^S)+\mathcal{T}(\vec{\boldsymbol{y}}^S,\vec{\boldsymbol{x}}_r),\vec{\boldsymbol{x}}_r;\vec{\boldsymbol{x}}_s\big),$$

where $\mathcal{T}(\vec{\boldsymbol{x}},\vec{\boldsymbol{y}})$ is an estimated travel time between the points $\vec{\boldsymbol{x}}$ and $\vec{\boldsymbol{y}}$. When the medium is homogeneous then

$$\mathcal{T}(\vec{\boldsymbol{x}},\vec{\boldsymbol{y}})=\frac{|\vec{\boldsymbol{x}}-\vec{\boldsymbol{y}}|}{c_0},$$

where c_0 is the constant propagation speed. In this case the images produced by Kirchhoff migration can be analyzed easily. For a point reflector the range resolution is c/B, where B is the bandwidth of the probing pulse, and the cross range resolution is $\lambda_0 L/a$, where λ_0 is the central wavelength of the pulse, L is the distance from the array to the reflector, and a is the size of the array. These are the Rayleigh resolution formulas [16]. When, however, the medium is inhomogeneous then migration may not work well. In weakly scattering media the images can be stabilized statistically by using coherent interferometry [9, 10, 11], which is a special correlation based imaging method. Statistical stability means high signal-to-noise ratio. In strongly scattering media we may be able to obtain an image by using special signal processing methods [8] but often we cannot get any image at all because the coherent signal from the

*Laboratoire de Probabilités et Modèles Aléatoires & Laboratoire Jacques-Louis Lions, Université Paris VII, site Chevaleret, 75205 Paris Cedex 13, France garnier@math.jussieu.fr

†Mathematics Department, Stanford University, Stanford, CA 94305 papanicolaou@stanford.edu

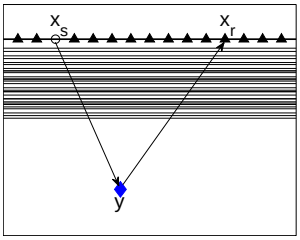

FIG. 1.1. *Sensor array imaging of a reflector located at $\vec{\boldsymbol{y}}$ through a scattering medium. $\vec{\boldsymbol{x}}_s$ is a source, $\vec{\boldsymbol{x}}_r$ is a receiver, and $\vec{\boldsymbol{y}}$ is a reflector.*

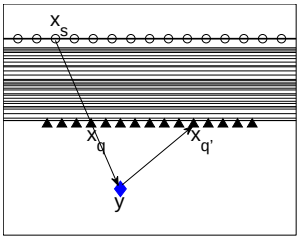

FIG. 1.2. *Use of an auxiliary passive array for imaging through a scattering medium. $\vec{\boldsymbol{x}}_s$ is a source, $\vec{\boldsymbol{x}}_q$ and $\vec{\boldsymbol{x}}_{q'}$ are two receivers located below the scattering medium, and $\vec{\boldsymbol{y}}$ is a reflector.*

reflector received at the array is very weak compared to the backscatter from the medium.

Consider now an imaging setup in which there is an auxiliary passive array, located at $(\vec{\boldsymbol{x}}_q)_{q=1}^{N_{\rm q}}$, and the strongly scattering medium is between it and the surface source-receiver array, as in Figure 1.2. Can the auxiliary passive array be used to get an image by mitigating the effects of the strong scattering between it and the surface source-receiver array? If we consider the strong scattering as producing signals that appear to come from spatially dispersed noisy sources, then we are in a daylight imaging setup with ambient noise sources, which was analyzed in [21]. Daylight imaging means illumination from behind the array. By analogy with the situation in which there are $N_{\rm s}$ uncorrelated point sources at $(\vec{\boldsymbol{x}}_s)_{s=1,\ldots,N_{\rm s}}$, we expect that, even in the case of active impulsive sources, the matrix of cross correlations at the auxiliary array

$$\mathcal{C}_T(\tau,\vec{\boldsymbol{x}}_q,\vec{\boldsymbol{x}}_{q'}) = \int_0^T \sum_{s=1}^{N_{\rm s}} p(t,\vec{\boldsymbol{x}}_q;\vec{\boldsymbol{x}}_s)p(t+\tau,\vec{\boldsymbol{x}}_{q'};\vec{\boldsymbol{x}}_s)dt\ , \qquad q,q'=1,\ldots,N_{\rm q}$$

behaves roughly as if it is the array response matrix of the auxiliary array. This means that it can be used for imaging with Kirchhoff migration:

$$\mathcal{I}(\vec{\boldsymbol{y}}^S) = \sum_{q,q'=1}^{N_{\rm q}} \mathcal{C}_T\big(\mathcal{T}(\vec{\boldsymbol{x}}_q,\vec{\boldsymbol{y}}^S) + \mathcal{T}(\vec{\boldsymbol{y}}^S,\vec{\boldsymbol{x}}_{q'}),\vec{\boldsymbol{x}}_q,\vec{\boldsymbol{x}}_{q'}\big).$$

In this paper we will show analytically the striking result that the resolution of the

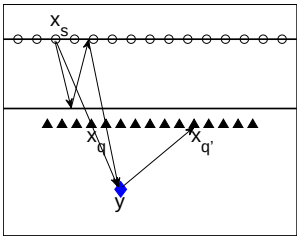

FIG. 1.3. *Sensor array imaging of a reflector located at $\vec{\boldsymbol{y}}$ in the presence of a strong interface that generates multiples by reverberation between the interface and the free surface.*

resulting images is given by the Rayleigh resolution formulas as if the medium was homogeneous [22]. This result is not obvious at all because scattering by inhomogeneities in the medium of waves emitted by the impulsive sources at the surface produces signals on the auxiliary passive array that are very different from those coming from spatially uncorrelated noise sources. This is especially true when addressing randomly layered media, which do not provide any lateral diversity enhancement since scattering does not change the transverse wavevectors. Nevertheless, it has been observed in exploration geophysics contexts [3, 35, 40] that imaging with the cross correlations of the auxiliary array is very effective and produces images that are nearly as good as in a homogeneous medium.

The first objective of this paper is to show analytically that for acoustic waves in randomly layered media, in a certain asymptotic regime which was studied in [18] and is described in Section 2, Kirchhoff migration images with cross correlations of the auxiliary array have the same resolution as those of a homogeneous medium. The reason why this kind of imaging works so well is because, by wave field reciprocity, the cross correlations $\mathcal{C}_T(\tau, \vec{\boldsymbol{x}}_q, \vec{\boldsymbol{x}}_{q'})$ can be given a time-reversal interpretation, which is well known [14], and then the analysis of time reversal refocusing in random media can be applied. The main results in time reversal in random media are (i) the enhanced refocusing, which means that the primary peak in the cross correlation will be observable only when the sensors in the auxiliary array are close enough with time lag close to zero, and then Kirchhoff migration to image the reflector will not be affected, and (ii) the statistical stability of the cross correlation function relative to the random medium inhomogeneities, provided that the source illumination from the surface is broadband (see [18, Chapters 12 and 15] and [17, 19]).

We also show in this paper, in Section 3, that when the auxiliary passive array is placed on or below a medium interface between the surface array and the reflector to be imaged, then Kirchhoff migration imaging with the auxiliary array cross correlations produces an image as if there is no interface (Figure 1.3). This is commonly encountered in exploration geophysics with marine surveys, where the surface source-receiver array is on the sea surface and the interface is at the bottom of the sea. The auxiliary array may be attached to the sea bottom and the reflectors to be imaged are underground. The problem addressed here, for a layered medium, is well-known in connection with the removal of multiple reflections from the sea surface and bottom in the data [2, 13].

In both randomly layered media and in media with a deterministic interface, it is expected [31] that decomposing the auxiliary array data into up and down going

wave signals and then calculating cross correlations only of the up going with the down going ones improves the Kirchhoff migration images. For the up and down going wave signal decomposition to be possible it is necessary to have both the pressure and the vertical velocity recorded at the array, or the three dimensional velocity. We quantify analytically in Section 2.6.3 the improvement in the Kirchhoff migration image.

What happens when the medium between the surface and the auxiliary array is not layered and is weakly, not strongly scattering so that backscattering can be neglected? In this case Kirchhoff migration with cross correlations of the auxiliary array produces images again as if the medium were homogeneous and the auxiliary array were active. Using the paraxial or parabolic approximation [28, 38, 39, 26, 27, 15, 23], we explain why this is so in Section 4. This shows that, although the technical details in the randomly layered case and in the random paraxial case are very different from each other, the final result is the same. We therefore expect that this result holds for a broad class of random media. In particular, if the medium between the surface and the auxiliary array is isotropically strongly scattering then it is not known (from the theoretical point of view) if imaging with cross correlations of the auxiliary array is effective. However, it is expected that it will be considerably better than imaging directly with the surface source-receiver array.

How do we image when the medium between the auxiliary array and the reflector is scattering, a randomly inhomogeneous medium? If the scattering is weak, then we can use cross correlations of the auxiliary array to form a coherent interferometric image, which amounts to using special fourth order cross correlations. This type of imaging was introduced in [9] and while some resolution is lost compared to a homogeneous medium, the images are statistically stable, that is, they tend not to depend on the realization of the random medium. The gain in signal-to-noise ratio in coherent interferometry compared to Kirchhoff migration is analyzed in [7] where it is shown that it can be quite significant. Of course, when the scattering is strong between the auxiliary array and the reflector it is unlikely that any image can be formed.

2. Imaging through a Randomly Layered Medium.

2.1. Acoustic Model. In this section we consider linear acoustic waves propagating in a three-dimensional layered medium and generated by a point source. Motivated by geophysical applications, we take a typical wavelength of the probing pulse to be larger than the correlation length of the medium and smaller than the propagation distance. This is the regime studied for instance in [1, 18] and is appropriate in exploration geophysics [41], in which the correlation length l_c is estimated to be $2-3$m, the central wavelength λ is 150m, and the propagation distance L is typically $5-10$km. This corresponds to a peak frequency of 50Hz and with a mean speed of propagation 3km/sec. In the analysis we abstract this regime of physical parameters by introducing dimensionless parameter ε that captures roughly the ordering of the scaling ratios:

$$\frac{l_c}{L} \sim \varepsilon^2, \qquad \frac{\lambda}{L} \sim \varepsilon. \tag{2.1}$$

As is the case when asymptotic theories are applied to physical problems, what is essential here is that (i) the mathematical scaling is broadly compatible with the physical parameters, and (ii) the cumulative effects of multiple scattering by the random inhomogeneities upon the propagating waves are significant and captured by the analysis.

The governing equations for the acoustic waves are

$$\rho^\varepsilon(z)\frac{\partial \vec{\boldsymbol{u}}^\varepsilon}{\partial t} + \nabla p^\varepsilon = \vec{\boldsymbol{F}}^\varepsilon(t,\vec{\boldsymbol{x}}), \qquad \frac{1}{K^\varepsilon(z)}\frac{\partial p^\varepsilon}{\partial t} + \nabla\cdot\vec{\boldsymbol{u}}^\varepsilon = 0, \tag{2.2}$$

where p^ε is the pressure field, $\vec{\boldsymbol{u}}^\varepsilon$ is the three-dimensional velocity field, ρ^ε is the density of the medium, K^ε is the bulk modulus of the medium, and $\vec{\boldsymbol{x}} = (\boldsymbol{x}, z) \in \mathbb{R}^2\times\mathbb{R}$ are the space coordinates. The parameters of the medium ρ^ε and K^ε vary only along the z-direction. The forcing term $\vec{\boldsymbol{F}}^\varepsilon$ models the source located just below the surface $z = 0$.

We consider in this section the situation in which a layered medium occupies the section $z \in (-L, 0)$ and is sandwiched in between two homogeneous half-spaces. The homogeneous half-space $z \le -L$ is matched to the layered section $z \in (-L, 0)$ (we will consider the un-matched case in Section 3). Motivated by geophysical applications we assume that the density ρ_a in the homogeneous half-space $z \ge 0$ is much smaller than the density $\rho^\varepsilon(z)$ in the layered medium for $z \le 0$. Since the velocity and pressure are continuous, the pressure in $z > 0$ goes to zero and hence, by continuity, also at $z = 0$. These are the so-called pressure release boundary conditions: $p^\varepsilon(t, (\boldsymbol{x}, z = 0)) = 0$.

We consider the case with a randomly layered medium in the region $z \in (-L, 0)$. The parameters of the medium are assumed to be of the form

$$\left(K^\varepsilon\right)^{-1}(z) = \begin{cases} K_0^{-1} & \text{if } z \in (-\infty, -L] \\ K_0^{-1}[1 + \nu(\frac{z}{\varepsilon^2})] & \text{if } z \in (-L, 0) \end{cases}, \tag{2.3}$$

$$\rho^\varepsilon(z) = \rho_0 \quad \text{if } z \in (-\infty, 0). \tag{2.4}$$

In this model the parameters of the medium have random and rapid fluctuations with a typical scale of variation much smaller than the thickness of the layer. The small dimensionless parameter ε^2 is the ratio between these two scales. The small-scale random fluctuations are described by the random process $\nu(z)$. The process ν is bounded in magnitude by a constant less than one, so that K^ε is a positive quantity. The random process $\nu(z)$ is stationary and zero mean. It is supposed to have strong mixing properties so that we can use averaging techniques for stochastic differential equations as presented in [18, Chapter 6]. The important quantity from the statistical point of view is the integrated covariance of the fluctuations of the random medium defined by

$$\gamma = \int_{-\infty}^{\infty} \mathbb{E}[\nu(z')\nu(z'+z)]dz. \tag{2.5}$$

By the Wiener-Khintchine theorem it is nonnegative valued as it is the power spectral density evaluated at zero-frequency. The integrated covariance γ plays the role of scattering coefficient. It is of the order of the product of the variance of the medium fluctuations times the correlation length of the medium fluctuations. As will become clear in the sequel, the statistics of the wave field depend on the random medium via this integrated covariance or power spectral density.

The source is modeled by the forcing term $\vec{\boldsymbol{F}}^\varepsilon$. We assume that it is point-like, located at $\vec{\boldsymbol{x}}_s = (\boldsymbol{x}_s, 0^-)$, i.e. just below the surface $z = 0$, and that it emits a short pulse whose central wavelength is of order ε:

$$\vec{\boldsymbol{F}}^\varepsilon(t,\boldsymbol{x},z) = \vec{\boldsymbol{f}}^\varepsilon(t)\delta(z)\delta(\boldsymbol{x}-\boldsymbol{x}_s), \qquad \vec{\boldsymbol{f}}^\varepsilon(t) = \varepsilon\vec{\boldsymbol{f}}\Big(\frac{t}{\varepsilon}\Big), \tag{2.6}$$

where we assume that the support of the Fourier transform of $\vec{\boldsymbol{f}} = (\boldsymbol{f}_{\boldsymbol{x}}, f_z)$ is bounded away from zero and of rapid decay at infinity. The particular scaling of $\vec{\boldsymbol{f}}^{\varepsilon}$ in (2.6) means that the central wavelength is large compared to the microscopic scale of variation of the random fluctuations of the medium and small compared to the macroscopic scale of variation of the background medium, as in (2.1). The normalizing amplitude factor ε multiplying the source term is not important as the wave equation is linear, but it will make the quantities of interest of order one as $\varepsilon \to 0$, which explains our choice.

We define the background velocity and impedance by

$$c_0 = \frac{\sqrt{K_0}}{\sqrt{\rho_0}}, \qquad \zeta_0 = \sqrt{K_0 \rho_0}. \tag{2.7}$$

2.2. Review of Wave Propagation in Randomly Layered Media. A randomly layered medium is a model that is both mathematically tractable and physically relevant. In this paper we will give some precise results but we would like to give a few qualitative results in this subsection [18, Chapter 7]. If we consider a plane wave $\hat{p}^{\varepsilon}_{\rm inc}(\omega, z) = \exp(i\varepsilon\omega z)$ with frequency $\varepsilon\omega$ normally incident to a randomly layered medium with matched boundary conditions, then the transmission coefficient $T^{\varepsilon}(\omega)$ describes how the wave is transmitted through the random medium $\hat{p}^{\varepsilon}_{\rm tr}(\omega, z) = T^{\varepsilon}(\omega)\exp(i\varepsilon\omega z)$.

The mean transmission coefficient $\mathbb{E}[T^{\varepsilon}]$ gives the behavior of the coherent components of the transmitted wave. The analysis shows that it decays exponentially with the size of the random medium with the rate $\exp(-L/l_{\rm sca})$ where $l_{\rm sca} = 4c_0^2/(\omega^2\gamma)$ is called the scattering mean free path in the physical literature. This is the result of an exponential decay of the amplitude and a random phase that averages out to enhance the decay of the expectation $\mathbb{E}[T^{\varepsilon}]$.

The mean power transmission coefficient $\mathbb{E}[|T^{\varepsilon}|^2]$ gives the behavior of the incoherent components of the transmitted wave. The analysis shows that it decays exponentially with the rate $\exp(-2L/l_{\rm loc})$ where $l_{\rm loc} = 32c_0^2/(\omega^2\gamma)$ is called the localization length in the physical literature. In a randomly layered medium the localization length and the scattering mean free path are proportional in the regime described in the previous subsection, but this is not true for other types of random media. Note that, in the regime $L > l_{\rm loc}$, the coherent transmitted wave energy $|\mathbb{E}[T^{\varepsilon}]|^2$ is much smaller than the incoherent transmitted wave energy $\mathbb{E}[|T^{\varepsilon}|^2]$.

In this paper we have in mind the regime in which the size of the random medium is larger than the scattering mean free path, which means that there is almost no coherent wave transmitted through the random medium. As a first consequence, migration of the recorded fields will not give good images in a situation such as in Figure 1.2, because migration only uses coherent information. As a second consequence the waves being transmitted through the random medium and going through the auxiliary array are incoherent (although they still present some correlation structure since scattering by a randomly layered medium does not enhance lateral diversity). By analogy with ambient noise imaging, we anticipate that migration of cross correlations will produce good images.

2.3. The Main Results about Migration Imaging. The calculation of the empirical cross correlation at two receivers $\vec{\boldsymbol{x}}_q = (\boldsymbol{x}_q, -L)$ and $\vec{\boldsymbol{x}}_{q'} = (\boldsymbol{x}_{q'}, -L)$ of the auxiliary array located at depth $z = -L$ is carried out as follows:
1) For a given point source at $\vec{\boldsymbol{x}}_s = (\boldsymbol{x}_s, 0)$, the pressure fields are recorded at the two

receivers $\vec{\boldsymbol{x}}_q$ and $\vec{\boldsymbol{x}}_{q'}$ and the cross correlation between these fields is computed:

$$C^\varepsilon(\tau, \vec{\boldsymbol{x}}_q, \vec{\boldsymbol{x}}_{q'}; \boldsymbol{x}_s) = \int p^\varepsilon(t, \vec{\boldsymbol{x}}_q; \vec{\boldsymbol{x}}_s) p^\varepsilon(t+\tau, \vec{\boldsymbol{x}}_{q'}; \vec{\boldsymbol{x}}_s) dt. \tag{2.8}$$

2) The cross correlations are summed over all point sources. Assuming a dense source array (sampled at the scale of the wavelength) covering the whole surface $z = 0$, we obtain the following cross correlation (the wavelength being of order ε):

$$\mathcal{C}^\varepsilon(\tau, \vec{\boldsymbol{x}}_q, \vec{\boldsymbol{x}}_{q'}) = \varepsilon^{-2} \int C^\varepsilon(\tau, \vec{\boldsymbol{x}}_q, \vec{\boldsymbol{x}}_{q'}; \boldsymbol{x}_s) d\boldsymbol{x}_s. \tag{2.9}$$

In this subsection we assume that a small reflector is buried below the random medium at position $\vec{\boldsymbol{y}} = (\boldsymbol{y}, -L_y)$. We use the Born approximation to describe the interaction of the wave field with the reflector (see Subsection 2.5.2). We give in Subsections 2.3.1-2.3.3 the main results of this paper which are proved in Sections 2.6-2.7.

2.3.1. Migration of the Cross Correlation Matrix of the Auxiliary Array Data. The Kirchhoff migration function for the search point $\vec{\boldsymbol{y}}^S$ is

$$\mathcal{I}^\varepsilon_{\mathrm{C}}(\vec{\boldsymbol{y}}^S) = \frac{1}{N_{\mathrm{q}}^2} \sum_{q,q'=1}^{N_{\mathrm{q}}} \mathcal{C}^\varepsilon\Big(\frac{|\vec{\boldsymbol{x}}_q - \vec{\boldsymbol{y}}^S| + |\vec{\boldsymbol{y}}^S - \vec{\boldsymbol{x}}_{q'}|}{c_0}, \vec{\boldsymbol{x}}_q, \vec{\boldsymbol{x}}_{q'}\Big), \tag{2.10}$$

where N_{q} is the number of receivers at the auxiliary array.

PROPOSITION 2.1. *If the receiver array at depth $-L$ is a dense square array centered at $\boldsymbol{x}_A$ and with sidelength a (i.e. the distance between the sensors is smaller than or equal to half-a-central wavelength), then, denoting the search point by*

$$\vec{\boldsymbol{y}}^S = \vec{\boldsymbol{y}} + (\boldsymbol{\xi}, \eta),$$

we have

$$\begin{aligned}\mathcal{I}^\varepsilon_{\mathrm{C}}(\vec{\boldsymbol{y}}^S) \overset{\varepsilon\to 0}{\longrightarrow} & \frac{i\sigma_{\mathrm{ref}}}{2(2\pi)^3 c_0^3 (L_y - L)^2} \mathrm{sinc}^2\Big(\frac{\pi a \xi_1}{\lambda_0(L_y - L)}\Big) \mathrm{sinc}^2\Big(\frac{\pi a \xi_2}{\lambda_0(L_y - L)}\Big) \\ & \times \int \omega^3 |\hat{f}_z(\omega)|^2 \exp\Big(2i\frac{\omega}{c_0}(\eta + \boldsymbol{\xi} \cdot \frac{\boldsymbol{x}_A - \boldsymbol{y}}{L_y - L})\Big) d\omega.\end{aligned} \tag{2.11}$$

Here σ_{ref} is the scattering cross section of the reflector. $\hat{f}_z$ is the Fourier transform of the source pulse

$$\hat{f}_z(\omega) = \int f_z(t) e^{i\omega t} dt.$$

The central wavelength is defined by $\lambda_0 = 2\pi c_0/\omega_0$ where ω_0 is the central frequency of the source pulse. In order to simplify the expression we have assumed the following hypothesis:

$$\begin{aligned}&\text{The sidelength } a \text{ is smaller than the depth } L_y - L. \\ &\text{The bandwidth } B \text{ of the source pulse is small compared} \\ &\text{ to the central frequency } \omega_0.\end{aligned} \tag{2.12}$$

Note that the result is not changed quantitatively if a is of the same order as or larger than $L_y - L$ or if the bandwidth is of the same order as the central frequency, but then the transverse shape is not a sinc anymore.

This shows that
- The migration of the cross correlation gives the same result as if we were migrating the array response matrix of the auxiliary array. Indeed the imaging function (2.11) is almost exactly the imaging function that we would obtain if the medium were homogeneous, if the auxiliary receiver array could be used as an active array, and if the response matrix of the auxiliary array were migrated to the search point $\boldsymbol{y}^S$ (see Appendix B). In particular the cross range resolution is $\lambda_0(L-L_y)/a$ and the range resolution is c_0/B.
- Although the coherent components of the waves that illuminate the region of interest $z<-L$ through the array are exponentially damped and have random wavefront distortions, the cross correlation technique efficiently uses all the coherent and incoherent components that illuminate the region of interest.

In contrast, we state in the next subsections that migration of signals recorded by the surface array or by the auxiliary array does not give good images.

2.3.2. Migration of the Surface Array Data. The data set is here the signals (vertical velocity fields) recorded at the surface at points $\vec{\boldsymbol{x}}_r=(\boldsymbol{x}_r,0)$ and emitted by a point source at $\vec{\boldsymbol{x}}_s=(\boldsymbol{x}_s,0)$. The Kirchhoff migration function for the search point $\vec{\boldsymbol{y}}^S$ is

$$\mathcal{I}^{\varepsilon}_{\rm S}(\vec{\boldsymbol{y}}^S)=\frac{1}{N_{\rm s}N_{\rm r}}\sum_{s=1}^{N_{\rm s}}\sum_{r=1}^{N_{\rm r}}u^{\varepsilon}\Big(\frac{|\vec{\boldsymbol{x}}_s-\vec{\boldsymbol{y}}^S|+|\vec{\boldsymbol{y}}^S-\vec{\boldsymbol{x}}_r|}{c_0},\vec{\boldsymbol{x}}_r;\vec{\boldsymbol{x}}_s\Big), \tag{2.13}$$

where $N_{\rm s}$ is the number of sources and $N_{\rm r}$ is the number of observation points at the surface.

If the source and receiver arrays at the surface $z=0$ are a dense array that covers completely the surface, then, denoting the search point by $\vec{\boldsymbol{y}}^S=\vec{\boldsymbol{y}}+(\boldsymbol{\xi},\eta)$, we have

$$\begin{aligned}\mathcal{I}^{\varepsilon}_{\rm S}(\vec{\boldsymbol{y}}^S)\stackrel{\varepsilon\to 0}{\longrightarrow}&\frac{i\sigma_{\rm ref}L_y^2}{2(2\pi)\big(\frac{\gamma\omega_0^2}{4c_0^2}L-i\omega_0\frac{\sqrt{\gamma}}{\sqrt{2}c_0}W_0(L)\big)^2}\exp\Big[-\frac{\omega_0^2|\boldsymbol{\xi}|^2}{c_0^2\big(\frac{\gamma\omega_0^2}{4c_0^2}L-i\omega_0\frac{\sqrt{\gamma}}{2\sqrt{2}c_0}W_0(L)\big)}\Big]\\&\times\int\omega^3\hat{f}_z(\omega)\exp\Big(2i\frac{\omega}{c_0}\big(\eta+\frac{\sqrt{\gamma}}{2\sqrt{2}c_0}W_0(L)\big)\Big)\exp\Big(-\frac{\gamma\omega^2}{4c_0^2}L\Big)d\omega,\end{aligned} \tag{2.14}$$

where $W_0(L)$ is a Gaussian random variable with mean zero and variance L. Here we have assumed that the damping due to the random fluctuations is relatively strong $\omega_0^2\gamma L/c_0^2>1$ and that the bandwidth B of the probing pulse is small compared to the central frequency ω_0.

Compared to the imaging function using the cross correlation matrix, and due to the fact that the usual imaging function only uses the coherent wave components, we observe:
- an exponential damping, more exactly, a spreading by a Gaussian convolution kernel, which reduces both the range resolution and the signal-to-noise ratio,
- an error in the range estimation due to random wavefront distortions. More exactly, the range identification is wrong by a random shift given by $-\sqrt{\gamma}W_0(L)/\sqrt{8}$,
- the focal spot shape is not deterministic but random.

2.3.3. Migration of the Auxiliary Array Data. The data set is here the signals (pressure fields or vertical velocity fields) recorded at the auxiliary passive array at points $\vec{\boldsymbol{x}}_q=(\boldsymbol{x}_q,-L)$ and emitted by a point source at $\vec{\boldsymbol{x}}_s=(\boldsymbol{x}_s,0)$. This

is exactly the same data set as the one used in the function (2.10). The Kirchhoff migration function for the search point $\vec{\boldsymbol{y}}^S$ is

$$\mathcal{I}^{\varepsilon}_{\mathrm{R}}(\vec{\boldsymbol{y}}^S) = \frac{1}{N_{\mathrm{s}}N_{\mathrm{q}}}\sum_{s=1}^{N_{\mathrm{s}}}\sum_{q=1}^{N_{\mathrm{q}}} p^{\varepsilon}\Big(\frac{|\vec{\boldsymbol{x}}_s-\vec{\boldsymbol{y}}^S|+|\vec{\boldsymbol{y}}^S-\vec{\boldsymbol{x}}_q|}{c_0},\vec{\boldsymbol{x}}_q;\vec{\boldsymbol{x}}_s\Big), \tag{2.15}$$

where N_{s} is the number of sources at the surface and N_{q} is the number of receivers in the auxiliary passive array.

If the source array at the surface $z=0$ is a dense array that covers completely the surface and if the auxiliary receiver array is a dense square array centered at $\boldsymbol{x}_A$ and with sidelength a, then, denoting the search point by $\vec{\boldsymbol{y}}^S=\vec{\boldsymbol{y}}+(\boldsymbol{\xi},\eta)$, we have

$$\begin{aligned}\mathcal{I}^{\varepsilon}_{\mathrm{R}}(\vec{\boldsymbol{y}}^S) \overset{\varepsilon\to 0}{\longrightarrow} & -\frac{i\sigma_{\mathrm{ref}}L_y}{2(2\pi)^2(L_y-L)\big(\frac{\gamma\omega_0^2}{4c_0^2}L-i\omega_0\frac{\sqrt{\gamma}}{2c_0}W_0(L)\big)}\\ &\times\mathrm{sinc}\Big(\frac{a\xi_1\omega_0}{2c_0(L_y-L)}\Big)\mathrm{sinc}\Big(\frac{a\xi_2\omega_0}{2c_0(L_y-L)}\Big)\exp\Big[-\frac{\omega_0^2|\boldsymbol{\xi}|^2}{c_0^2\big(\frac{\gamma\omega_0^2}{2c_0^2}L-i\omega_0\frac{\sqrt{\gamma}}{c_0}W_0(L)\big)}\Big]\\ &\times\int\omega^3\hat{f}_z(\omega)\exp\Big(i\frac{\omega}{c_0}\big(2\eta+\boldsymbol{\xi}\cdot\frac{\boldsymbol{x}_A-\boldsymbol{y}}{L_y-L}+\frac{\sqrt{\gamma}}{2}W_0(L)\big)\Big)\exp\Big(-\frac{\gamma\omega^2}{8c_0^2}L\Big)d\omega.\end{aligned} \tag{2.16}$$

In order to simplify the expression we have here assumed Hypothesis (2.12) and we have assumed that the damping due to the random fluctuations is strong $\omega_0^2\gamma L/c_0^2>1$.

Compared to the imaging function using the cross correlation matrix, and due to the fact that the usual imaging function only uses the coherent wave components, we observe:
- an exponential damping, more exactly, a spreading by a Gaussian convolution kernel, which reduces both the range resolution and the signal-to-noise ratio,
- an error in the range estimation due to random wavefront distortions. More exactly, the range identification is wrong by a random shift given by $-\sqrt{\gamma}W_0(L)/4$,
- the focal spot is not always deterministic but it can be random, if the Gaussian in $\boldsymbol{\xi}$ dominates the sinc functions in (2.16), which happens if the receiver array is too small: $a^2<c_0^2(L_y-L)^2/(\gamma\omega_0^2L)$.

2.4. The Field in the Absence of a Reflector. In this section we analyze the wave transmitted through a randomly layered medium when there is no embedded reflector.

2.4.1. Integral Representation of the Field. When there is a point source at $\vec{\boldsymbol{x}}_s=(\boldsymbol{x}_s,0)$ (see Figure 2.1) the pressure field recorded at some point $\vec{\boldsymbol{x}}=(\boldsymbol{x},z)$ below the random medium $z\le -L$ has the integral representation

$$p^{\varepsilon}(t,\vec{\boldsymbol{x}};\vec{\boldsymbol{x}}_s) = -\frac{1}{(2\pi)^3\varepsilon}\int\hat{f}_z(\omega)\mathcal{G}^{\varepsilon}_{\omega,\kappa}\exp\Big(-i\frac{\omega}{\varepsilon}\big(t-\boldsymbol{\kappa}\cdot(\boldsymbol{x}-\boldsymbol{x}_s)+\frac{z}{c_0(\kappa)}\big)\Big)\omega^2 d\boldsymbol{\kappa}d\omega. \tag{2.17}$$

This expression is proved in Appendix A.1. Similarly, the vertical velocity field is

$$u^{\varepsilon}(t,\vec{\boldsymbol{x}};\vec{\boldsymbol{x}}_s) = \frac{1}{(2\pi)^3\varepsilon}\int\frac{\hat{f}_z(\omega)}{\zeta_0(\kappa)}\mathcal{G}^{\varepsilon}_{\omega,\kappa}\exp\Big(-i\frac{\omega}{\varepsilon}\big(t-\boldsymbol{\kappa}\cdot(\boldsymbol{x}-\boldsymbol{x}_s)+\frac{z}{c_0(\kappa)}\big)\Big)\omega^2 d\boldsymbol{\kappa}d\omega. \tag{2.18}$$

Here, we have used the notation $\kappa=|\boldsymbol{\kappa}|$, and:

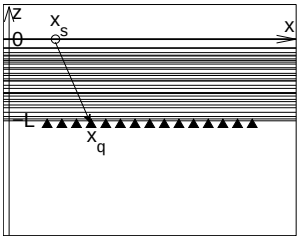

FIG. 2.1. *Emission from a point source located at* $\vec{\boldsymbol{x}}_s = (\boldsymbol{x}_s, 0)$ *in the surface array. The receiver is located at* $\vec{\boldsymbol{x}}_q = (\boldsymbol{x}_q, -L)$ *in the auxiliary array. The medium is random in the region* $z \in (-L, 0)$.

• The Fourier transforms are defined by

$$\hat{f}_z(\omega) = \int f_z(t) e^{i\omega t} dt.$$

• $\zeta_0(\kappa)$ and $c_0(\kappa)$ are the mode-dependent impedance and velocity

$$\zeta_0(\kappa) = \frac{\zeta_0}{\sqrt{1-\kappa^2 c_0^2}}, \qquad c_0(\kappa) = \frac{c_0}{\sqrt{1-\kappa^2 c_0^2}}. \tag{2.19}$$

• The random complex coefficient $\mathcal{G}^\varepsilon_{\omega,\kappa}$ is the Fourier-transformed Green's function (for pressure release boundary conditions). Here the Fourier transform is taken both with respect to time and with respect to the transverse spatial variables. The Green's function captures the interaction of the wave with the medium, both the scattering and the pressure release boundary conditions. It can be expressed in terms of the mode-dependent reflection and transmission coefficients $R^\varepsilon_{\omega,\kappa}$ and $T^\varepsilon_{\omega,\kappa}$ of the random section (for matched boundary conditions, that is, transparent boundary conditions), which are described in detail in Appendix A.1 (see Figure A.2) in the following way:

$$\mathcal{G}^\varepsilon_{\omega,\kappa} = \frac{T^\varepsilon_{\omega,\kappa}}{1 - R^\varepsilon_{\omega,\kappa}}. \tag{2.20}$$

We describe the statistical properties of the Green's function $\mathcal{G}^\varepsilon_{\omega,\kappa}$ in Section 2.6.1. We remark that the expansion

$$\mathcal{G}^\varepsilon_{\omega,\kappa} = \sum_{j=0}^{\infty} T^\varepsilon_{\omega,\kappa} (R^\varepsilon_{\omega,\kappa})^j$$

reflects the physical situation that the waves recorded at the bottom surface $z = -L$ are the sum of the contributions of the waves that have been transmitted through the random medium from the source plane $z = 0$ to the bottom surface $z = -L$ (term $j = 0$) and the contributions of the waves that have been reflected back and forth by the top surface and by the random region generating "multiples", until they eventually reach the bottom surface (see Figure 2.2). These reflections and multiples arise because of the pressure release boundary conditions at the surface which are an important aspect in the model in geophysical applications.

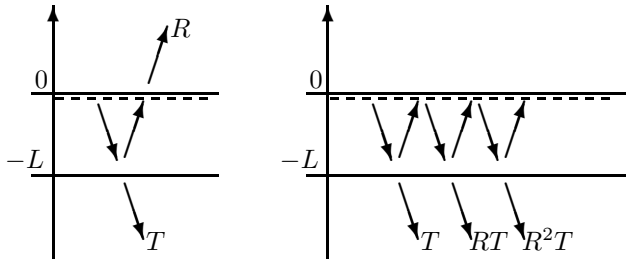

FIG. 2.2. *Schematic of the geometric configuration: The source is in the plane $z = 0$, the medium is random in the section $z \in (-L, 0)$, and the interface $z = 0$ is transparent (left, matched boundary conditions) or reflecting (right, pressure release boundary conditions). R, resp. T, is the reflection, resp. transmission, coefficient of the random medium.*

• The integrals in $\boldsymbol{\kappa}$ in (2.17-2.18) are limited to $\kappa < c_0^{-1}$. Modes generated with transverse slownesses that violate this condition are exponentially damped, so they can be neglected. Recall that the random medium is layered so that scattering does not change the slowness vector. In fact, we can limit the integral in $\boldsymbol{\kappa}$ to a smaller domain $\kappa < c_0^{-1} - \delta$, for some $\delta > 0$ because the travel time for mode $\boldsymbol{\kappa}$ to go from 0 to $-L$ is $Lc_0(\kappa)/c_0^2$. Therefore, if the time of the experiment is limited to T, then only the modes with $\kappa < c_0^{-1}(1 - c_0^2T^2/L^2)^{1/2}$ can be recorded at the surface $z = -L$. This limitation will allow us to neglect the contributions of the grazing modes (those with κ close to c_0^{-1}) and to avoid other technical difficulties.

2.4.2. Special Case with a Homogeneous Medium. In this section we consider the particular case when there is no random medium so that $\nu = 0$. The pressure field recorded at the point $\vec{\boldsymbol{x}}_q = (\boldsymbol{x}_q, -L)$ at depth $z = -L$ then has the integral representation (see Appendix A.1):

$$p^\varepsilon(t, \vec{\boldsymbol{x}}_q; \vec{\boldsymbol{x}}_s) = -\frac{1}{(2\pi)^3\varepsilon}\int \hat{f}_z(\omega)\exp\Big(-i\frac{\omega}{\varepsilon}\big(t-\boldsymbol{\kappa}\cdot(\boldsymbol{x}_q-\boldsymbol{x}_s)-i\frac{L}{c_0(\kappa)}\big)\Big)\omega^2 d\boldsymbol{\kappa}d\omega. \quad (2.21)$$

We consider here the limit $\varepsilon \to 0$. In the absence of microscopic random fluctuations of the medium this is simply a high-frequency regime. We now exploit this to obtain a simplified expression for the transmitted field by applying the stationary phase method [18, Chapter 14]. We find that the leading order value for the integral (2.21) is given by the contribution around the stationary slowness vector

$$\boldsymbol{\kappa}_{\rm sp} = \frac{1}{c_0}\frac{\boldsymbol{x}_q - \boldsymbol{x}_s}{\sqrt{L^2 + |\boldsymbol{x}_q - \boldsymbol{x}_s|^2}},$$

and this gives a contribution that is concentrated around the critical time

$$t_{\rm sp} = \frac{\sqrt{L^2 + |\boldsymbol{x}_q - \boldsymbol{x}_s|^2}}{c_0} = \frac{|\vec{\boldsymbol{x}}_q - \vec{\boldsymbol{x}}_s|}{c_0},$$

that is, the travel time from the source to the observation point. We find that the wave energy at $\vec{\boldsymbol{x}}_q$ arrives only around the travel time $|\vec{\boldsymbol{x}}_q - \vec{\boldsymbol{x}}_s|/c_0$ in the form of a short pulse:

$$\lim_{\varepsilon\to 0} p^\varepsilon\Big(\frac{|\vec{\boldsymbol{x}}_q - \vec{\boldsymbol{x}}_s|}{c_0} + \varepsilon s, \vec{\boldsymbol{x}}_q; \vec{\boldsymbol{x}}_s\Big) = -\frac{L}{2\pi c_0|\vec{\boldsymbol{x}}_q - \vec{\boldsymbol{x}}_s|^2}f_z'(s), \quad (2.22)$$

where the prime stands for time-derivative. This is characteristic of wave propagation in homogeneous media in the high-frequency regime.

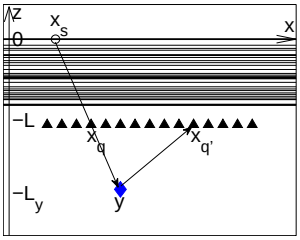

FIG. 2.3. *Emission from a point source located at* $\vec{\boldsymbol{x}}_s = (\boldsymbol{x}_s, 0)$. *The reflector position is* $\vec{\boldsymbol{y}} = (\boldsymbol{y}, -L_y)$. *The receivers are located at depth* $-L$: $\vec{\boldsymbol{x}}_q = (\boldsymbol{x}_q, -L)$ *and* $\vec{\boldsymbol{x}}_{q'} = (\boldsymbol{x}_{q'}, -L)$. *The medium is random in the region* $z \in (-L, 0)$.

2.5. The Field in the Presence of an Embedded Reflector. We consider the same situation as in Section 2.4 but with a reflector placed below the random medium. Figure 2.3 illustrates the geometry of the configuration: a point source is located at the top surface $\vec{\boldsymbol{x}}_s = (\boldsymbol{x}_s, 0)$, the reflector position is $\vec{\boldsymbol{y}} = (\boldsymbol{y}, -L_y)$, and the receivers are at depth $z = -L$: $\vec{\boldsymbol{x}}_q = (\boldsymbol{x}_q, -L)$, $\vec{\boldsymbol{x}}_{q'} = (\boldsymbol{x}_{q'}, -L)$.

We model the reflector as a local change in the density of the medium

$$\rho(\boldsymbol{x}, z) = \rho_0 + \rho_{\rm ref} \mathbf{1}_\Omega(\boldsymbol{x}, z)\,,$$

where Ω is a small domain around $\vec{\boldsymbol{y}}$. The system that governs the propagation of the acoustic waves can be written in the form

$$\begin{aligned} \rho_0 \frac{\partial \vec{\boldsymbol{u}}^\varepsilon}{\partial t} + \nabla p^\varepsilon &= \vec{\boldsymbol{F}}^\varepsilon - \rho_{\rm ref} \mathbf{1}_\Omega(\boldsymbol{x}, z) \frac{\partial \vec{\boldsymbol{u}}^\varepsilon}{\partial t}\,, \\ \frac{1}{K^\varepsilon(z)} \frac{\partial p^\varepsilon}{\partial t} + \nabla \cdot \vec{\boldsymbol{u}}^\varepsilon &= 0\,. \end{aligned}$$

2.5.1. The Born Approximation for an Embedded Reflector. We apply the Born approximation (or single-scattering approximation) for the modeling of the scattering by the reflector $\vec{\boldsymbol{y}}$ [32]: the total field

$$\vec{\boldsymbol{u}}^\varepsilon = \vec{\boldsymbol{u}}_0^\varepsilon + \vec{\boldsymbol{u}}_1^\varepsilon + \vec{\boldsymbol{u}}_r^\varepsilon\,, \qquad p^\varepsilon = p_0^\varepsilon + p_1^\varepsilon + p_r^\varepsilon \tag{2.23}$$

is the superposition of the primary field $(\vec{\boldsymbol{u}}_0^\varepsilon, p_0^\varepsilon)$ that solves

$$\begin{aligned} \rho_0 \frac{\partial \vec{\boldsymbol{u}}_0^\varepsilon}{\partial t} + \nabla p_0^\varepsilon &= \vec{\boldsymbol{F}}^\varepsilon\,, \\ \frac{1}{K^\varepsilon(z)} \frac{\partial p_0^\varepsilon}{\partial t} + \nabla \cdot \vec{\boldsymbol{u}}_0^\varepsilon &= 0\,, \end{aligned}$$

and of a secondary field $(\vec{\boldsymbol{u}}_1^\varepsilon, p_1^\varepsilon)$ that originates from the emission of a secondary source located at $\vec{\boldsymbol{y}}$. The emission of the secondary source is proportional to the primary field at the position of the reflector:

$$\rho_0 \frac{\partial \vec{\boldsymbol{u}}_1^\varepsilon}{\partial t} + \nabla p_1^\varepsilon = -\rho_{\rm ref} \mathbf{1}_\Omega(\boldsymbol{x}, z) \frac{\partial \vec{\boldsymbol{u}}_0^\varepsilon}{\partial t}\,, \tag{2.24}$$

$$\frac{1}{K^\varepsilon(z)} \frac{\partial p_1^\varepsilon}{\partial t} + \nabla \cdot \vec{\boldsymbol{u}}_1^\varepsilon = 0\,. \tag{2.25}$$

Both the primary and secondary fields satisfy the pressure release boundary conditions at $z = 0$. In the Born approximation the reminder $(\vec{\boldsymbol{u}}_r^\varepsilon, p_r^\varepsilon)$ is negligible (see Proposition 2.2 for conditions ensuring the validity of this approximation). Note that the Born approximation concerns only the interaction of the wave with the reflector at $\vec{\boldsymbol{y}}$. The multiple scattering of the wave with the random medium is taken into account.

2.5.2. Integral Expressions for the Wave Fields. We first consider the primary field $(\vec{\boldsymbol{u}}_0^\varepsilon, p_0^\varepsilon)$. The pressure field at the surface is zero $p_0^\varepsilon(t,(\boldsymbol{x},0);\vec{\boldsymbol{x}}_s) = 0$ and the vertical velocity field is

$$u_0^\varepsilon\big(t,(\boldsymbol{x},0);\vec{\boldsymbol{x}}_s\big) = \frac{1}{(2\pi)^3\varepsilon}\int \Big[\frac{1+R^\varepsilon_{\omega,\kappa}(-L,0)}{1-R^\varepsilon_{\omega,\kappa}(-L,0)}\frac{\hat f_z(\omega)}{2\zeta_0(\kappa)} + \frac{\boldsymbol{\kappa}\cdot\hat{\boldsymbol{f}}_{\boldsymbol{x}}(\omega)}{\rho_0}\Big] \times e^{-i\frac{\omega}{\varepsilon}(t-\boldsymbol{\kappa}\cdot(\boldsymbol{x}-\boldsymbol{x}_s))}\omega^2 d\omega\, d\boldsymbol{\kappa}\,, \quad (2.26)$$

as shown in Appendix A.2. The pressure and velocity fields at the position $\vec{\boldsymbol{x}} = (\boldsymbol{x}, z)$ below the random medium $(z \le -L)$ are given by:

$$p_0^\varepsilon(t,\vec{\boldsymbol{x}};\vec{\boldsymbol{x}}_s) = -\frac{1}{(2\pi)^3\varepsilon}\int \mathcal{G}^\varepsilon_{\omega,\kappa}(-L,0)e^{-i\frac{\omega}{\varepsilon}(t-\boldsymbol{\kappa}\cdot(\boldsymbol{x}-\boldsymbol{x}_s)+z/c_0(\kappa))}\hat f_z(\omega)\omega^2 d\omega d\boldsymbol{\kappa}\,, \quad (2.27)$$

$$u_0^\varepsilon(t,\vec{\boldsymbol{x}};\vec{\boldsymbol{x}}_s) = \frac{1}{(2\pi)^3\varepsilon}\int \frac{\mathcal{G}^\varepsilon_{\omega,\kappa}(-L,0)}{\zeta_0(\kappa)}e^{-i\frac{\omega}{\varepsilon}(t-\boldsymbol{\kappa}\cdot(\boldsymbol{x}-\boldsymbol{x}_s)+z/c_0(\kappa))}\hat f_z(\omega)\omega^2 d\omega d\boldsymbol{\kappa}\,, \quad (2.28)$$

$$\boldsymbol{v}_0^\varepsilon(t,\vec{\boldsymbol{x}};\vec{\boldsymbol{x}}_s) = -\frac{1}{(2\pi)^3\varepsilon}\int \frac{\boldsymbol{\kappa}\mathcal{G}^\varepsilon_{\omega,\kappa}(-L,0)}{\rho_0}e^{-i\frac{\omega}{\varepsilon}(t-\boldsymbol{\kappa}\cdot(\boldsymbol{x}-\boldsymbol{x}_s)+z/c_0(\kappa))}\hat f_z(\omega)\omega^2 d\omega d\boldsymbol{\kappa}\,, \quad (2.29)$$

where $\vec{\boldsymbol{u}}_0^\varepsilon = (\boldsymbol{v}_0^\varepsilon, u_0^\varepsilon)$, as shown in the previous section, and $\mathcal{G}^\varepsilon_{\omega,\kappa}$ is given by (2.20). The secondary field is described in the following proposition.

PROPOSITION 2.2. *When $\rho_{\rm ref}\mathrm{Vol}(\Omega) = \rho_0\sigma_{\rm ref}\varepsilon^2$ with $\sigma_{\rm ref} \ll 1$, then the Born approximation is valid and we have at the observation point $\vec{\boldsymbol{x}}_q = (\boldsymbol{x}_q, -L)$ (see Figure 2.3):*

$$p_1^\varepsilon(t,\vec{\boldsymbol{x}}_q;\vec{\boldsymbol{x}}_s) = \frac{i\sigma_{\rm ref}}{2(2\pi)^5\varepsilon^2}\int\left(-\frac{\zeta_0(\kappa)\boldsymbol{\kappa}\cdot\boldsymbol{\kappa}'}{\rho_0} + \frac{\rho_0}{\zeta_0(\kappa')}\right)\hat f_z(\omega)\omega^5\mathcal{G}^\varepsilon_{\omega,\kappa'} \times\Big[e^{i\frac{\omega}{\varepsilon}\phi_I(\boldsymbol{\kappa},\boldsymbol{\kappa}')} - \Big(\widetilde R^\varepsilon_{\omega,\kappa}(-L,0) + \frac{(T^\varepsilon_{\omega,\kappa}(-L,0))^2}{1-R^\varepsilon_{\omega,\kappa}(-L,0)}\Big)e^{i\frac{\omega}{\varepsilon}\phi_{II}(\boldsymbol{\kappa},\boldsymbol{\kappa}')}\Big]d\omega d\boldsymbol{\kappa} d\boldsymbol{\kappa}'\,, \quad (2.30)$$

where the two rapidly varying phases are

$$\phi_I(\boldsymbol{\kappa},\boldsymbol{\kappa}') = -t + \boldsymbol{\kappa}\cdot(\boldsymbol{x}_q-\boldsymbol{y}) + \frac{L_y-L}{c_0(\kappa)} + \boldsymbol{\kappa}'\cdot(\boldsymbol{y}-\boldsymbol{x}_s) + \frac{L_y}{c_0(\kappa')}\,, \quad (2.31)$$

$$\phi_{II}(\boldsymbol{\kappa},\boldsymbol{\kappa}') = -t + \boldsymbol{\kappa}\cdot(\boldsymbol{x}_q-\boldsymbol{y}) + \frac{L_y+L}{c_0(\kappa)} + \boldsymbol{\kappa}'\cdot(\boldsymbol{y}-\boldsymbol{x}_s) + \frac{L_y}{c_0(\kappa')}\,. \quad (2.32)$$

Here $\widetilde R^\varepsilon_{\omega,\kappa}(-L,0)$ is the adjoint mode-dependent reflection coefficient of the random section (for matched boundary conditions), which is described in Appendix A.4 (see Figure A.3).

Proof. We consider the secondary field solution of (2.24-2.25). We take a Fourier transform with respect to the time and the transverse spatial variables defined by

(A.1-A.2) to obtain

$$-\rho_0\frac{i\omega}{\varepsilon}\hat{\boldsymbol{v}}_1^\varepsilon + i\frac{\omega}{\varepsilon}\boldsymbol{\kappa}\hat{p}_1^\varepsilon = \rho_{\rm ref}\frac{i\omega}{\varepsilon}\int \boldsymbol{v}_0^\varepsilon(t,\boldsymbol{x},z)\mathbf{1}_\Omega(\boldsymbol{x},z)e^{i\frac{\omega}{\varepsilon}(t-\boldsymbol{\kappa}\cdot\boldsymbol{x})}\,dt\,d\boldsymbol{x}\,,$$

$$-\rho_0\frac{i\omega}{\varepsilon}\hat{u}_1^\varepsilon + \frac{\partial\hat{p}_1^\varepsilon}{\partial z} = \rho_{\rm ref}\frac{i\omega}{\varepsilon}\int u_0^\varepsilon(t,\boldsymbol{x},z)\mathbf{1}_\Omega(\boldsymbol{x},z)e^{i\frac{\omega}{\varepsilon}(t-\boldsymbol{\kappa}\cdot\boldsymbol{x})}\,dt\,d\boldsymbol{x}\,,$$

$$-\frac{1}{K^\varepsilon(z)}\frac{i\omega}{\varepsilon}\hat{p}_1^\varepsilon + i\frac{\omega}{\varepsilon}\boldsymbol{\kappa}\cdot\hat{\boldsymbol{v}}_1^\varepsilon + \frac{\partial\hat{u}_1^\varepsilon}{\partial z} = 0\,,$$

where $\vec{\boldsymbol{u}}_1^\varepsilon = (\boldsymbol{v}_1^\varepsilon, u_1^\varepsilon)$. We assume that the scattering region Ω is smaller than the wavelength, and we model it by a point reflector with scattering cross section of order $\varepsilon^2\sigma_{\rm ref}$, with $\sigma_{\rm ref}$ small, so that $\rho_{\rm ref}{\rm Vol}(\Omega) = \rho_0\sigma_{\rm ref}\varepsilon^2$ and

$$\rho_{\rm ref}\mathbf{1}_\Omega(\boldsymbol{x},z) = \varepsilon^2\rho_0\sigma_{\rm ref}\delta(\boldsymbol{x}-\boldsymbol{y})\delta(z+L_y)\,.$$

Therefore, the secondary field $(\vec{\boldsymbol{u}}_1^\varepsilon, p_1^\varepsilon)$ solves

$$-\rho_0\frac{i\omega}{\varepsilon}\hat{\boldsymbol{v}}_1^\varepsilon + i\frac{\omega}{\varepsilon}\boldsymbol{\kappa}\hat{p}_1^\varepsilon = \varepsilon^2\hat{\boldsymbol{f}}_{1,\boldsymbol{x}}^\varepsilon(\omega;\vec{\boldsymbol{x}}_s)e^{-i\frac{\omega}{\varepsilon}\boldsymbol{\kappa}\cdot\boldsymbol{y}}\delta(z+L_y)\,, \tag{2.33}$$

$$-\rho_0\frac{i\omega}{\varepsilon}\hat{u}_1^\varepsilon + \frac{\partial\hat{p}_1^\varepsilon}{\partial z} = \varepsilon^2\hat{f}_{1,z}^\varepsilon(\omega;\vec{\boldsymbol{x}}_s)e^{-i\frac{\omega}{\varepsilon}\boldsymbol{\kappa}\cdot\boldsymbol{y}}\delta(z+L_y)\,, \tag{2.34}$$

$$-\frac{1}{K^\varepsilon(z)}\frac{i\omega}{\varepsilon}\hat{p}_1^\varepsilon + i\frac{\omega}{\varepsilon}\boldsymbol{\kappa}\cdot\hat{\boldsymbol{v}}_1^\varepsilon + \frac{\partial\hat{u}_1^\varepsilon}{\partial z} = 0\,, \tag{2.35}$$

with the secondary source terms given by

$$\hat{\boldsymbol{f}}_{1,\boldsymbol{x}}^\varepsilon(\omega;\vec{\boldsymbol{x}}_s) = -\frac{i\sigma_{\rm ref}}{(2\pi)^2\varepsilon}\int \boldsymbol{\kappa}'\mathcal{G}_{\omega,\kappa'}^\varepsilon e^{i\frac{\omega}{\varepsilon}(\boldsymbol{\kappa}'\cdot(\boldsymbol{y}-\boldsymbol{x}_s)+L_y/c_0(\kappa'))}\hat{f}_z(\omega)\omega^3 d\boldsymbol{\kappa}'\,, \tag{2.36}$$

$$\hat{f}_{1,z}^\varepsilon(\omega;\vec{\boldsymbol{x}}_s) = \frac{i\sigma_{\rm ref}}{(2\pi)^2\varepsilon}\int \frac{\rho_0}{\zeta_0(\kappa')}\mathcal{G}_{\omega,\kappa'}^\varepsilon e^{i\frac{\omega}{\varepsilon}(\boldsymbol{\kappa}'\cdot(\boldsymbol{y}-\boldsymbol{x}_s)+L_y/c_0(\kappa'))}\hat{f}_z(\omega)\omega^3 d\boldsymbol{\kappa}'\,. \tag{2.37}$$

Note that the problem (2.33-2.35) has the same form as the system (2.38-2.40) for the primary field:

$$-\rho_0\frac{i\omega}{\varepsilon}\hat{\boldsymbol{v}}_0^\varepsilon + i\frac{\omega}{\varepsilon}\boldsymbol{\kappa}\hat{p}_0^\varepsilon = \varepsilon^2\hat{\boldsymbol{f}}_{\boldsymbol{x}}^\varepsilon(\omega)e^{-i\frac{\omega}{\varepsilon}\boldsymbol{\kappa}\cdot\boldsymbol{x}_s}\delta(z)\,, \tag{2.38}$$

$$-\rho_0\frac{i\omega}{\varepsilon}\hat{u}_0^\varepsilon + \frac{\partial\hat{p}_0^\varepsilon}{\partial z} = \varepsilon^2\hat{f}_z^\varepsilon(\omega)e^{-i\frac{\omega}{\varepsilon}\boldsymbol{\kappa}\cdot\boldsymbol{x}_s}\delta(z)\,, \tag{2.39}$$

$$-\frac{1}{K^\varepsilon(z)}\frac{i\omega}{\varepsilon}\hat{p}_0^\varepsilon + i\frac{\omega}{\varepsilon}\boldsymbol{\kappa}\cdot\hat{\boldsymbol{v}}_0^\varepsilon + \frac{\partial\hat{u}_0^\varepsilon}{\partial z} = 0\,, \tag{2.40}$$

but with a source term $\vec{\boldsymbol{f}}_1^\varepsilon$ that is now below the random medium.

It is easy to check from (2.36-2.37) that $\mathbb{E}[|\hat{\boldsymbol{f}}_{1,\boldsymbol{x}}^\varepsilon(\omega;\vec{\boldsymbol{x}}_s)|^2]$ and $\mathbb{E}[|\hat{f}_{1,z}^\varepsilon(\omega;\vec{\boldsymbol{x}}_s)|^2]$ are of order $\sigma_{\rm ref}^2$ uniformly in ε. In fact we have

$$\int \mathbb{E}[|\hat{\boldsymbol{f}}_{1,\boldsymbol{x}}^\varepsilon(\omega;\vec{\boldsymbol{x}}_s)|^2]d\boldsymbol{x}_s = \int \mathbb{E}[|\hat{f}_{1,z}^\varepsilon(\omega;\vec{\boldsymbol{x}}_s)|^2]d\boldsymbol{x}_s = \frac{\sigma_{\rm ref}^2\omega^2}{8\pi c_0^2}|\hat{f}_z(\omega)|^2.$$

The fact that the parameter $\sigma_{\rm ref}$ is small ensures the validity of the Born approximation, in the sense that in the expansion (2.23) we have

$$(\vec{\boldsymbol{u}}_0^\varepsilon, p_0^\varepsilon) \sim 1\,, \quad (\vec{\boldsymbol{u}}_1^\varepsilon, p_1^\varepsilon) \sim \sigma_{\rm ref}\,, \quad (\vec{\boldsymbol{u}}_r^\varepsilon, p_r^\varepsilon) \sim \sigma_{\rm ref}^2\,. \tag{2.41}$$

Let us consider the secondary pressure field p_1^ε at the observation point $\vec{\boldsymbol{x}}_q = (\boldsymbol{x}_q, -L)$ as illustrated in Figure 2.3. From the analysis carried out in Appendix A.4, we get

$$p_1^\varepsilon(t,\vec{\boldsymbol{x}}_q;\vec{\boldsymbol{x}}_s) = \frac{1}{(2\pi)^3\varepsilon}\int \frac{\sqrt{\zeta_0(\kappa)}}{2}\big[\hat a_1^\varepsilon(\omega,\boldsymbol{\kappa},-L)e^{-i\frac{\omega}{\varepsilon}L/c_0(\kappa)} - \hat b_1^\varepsilon(\omega,\boldsymbol{\kappa},-L)e^{i\frac{\omega}{\varepsilon}L/c_0(\kappa)}\big] \times e^{-i\frac{\omega}{\varepsilon}(t-\boldsymbol{\kappa}\cdot\boldsymbol{x}_q)}\omega^2 d\omega d\boldsymbol{\kappa}\,, \quad (2.42)$$

with

$$\hat a_1^\varepsilon(\omega,\boldsymbol{\kappa},-L) = \hat S_a^\varepsilon(\omega,\boldsymbol{\kappa})\,, \quad (2.43)$$

$$\hat b_1^\varepsilon(\omega,\boldsymbol{\kappa},-L) = \Big(\widetilde R^\varepsilon_{\omega,\kappa}(-L,0) + \frac{(T^\varepsilon_{\omega,\kappa}(-L,0))^2}{1-R^\varepsilon_{\omega,\kappa}(-L,0)}\Big)\hat S_a^\varepsilon(\omega,\boldsymbol{\kappa})\,, \quad (2.44)$$

$$\hat S_a^\varepsilon(\omega,\boldsymbol{\kappa}) = \Big[\frac{\sqrt{\zeta_0(\kappa)}}{\rho_0}\boldsymbol{\kappa}\cdot\hat{\boldsymbol{f}}^\varepsilon_{1,\boldsymbol{x}}(\omega;\vec{\boldsymbol{x}}_s) + \frac{1}{\sqrt{\zeta_0(\kappa)}}\hat f^\varepsilon_{1,z}(\omega;\vec{\boldsymbol{x}}_s)\Big]e^{i\frac{\omega}{\varepsilon}(-\boldsymbol{\kappa}\cdot\boldsymbol{y}+L_y/c_0(\kappa))}\,.$$

Thus, p_1^ε is given by (2.30). □

2.5.3. Matched Boundary Conditions At the Surface. The preasure release boundary conditions are appropriate for geophysical applications. In different contexts matched boundary conditions at the surface may be relevant. In this case, the results are modified as follows. The primary field at $\vec{\boldsymbol{x}}_q = (\boldsymbol{x}_q, -L)$ is

$$p_0^\varepsilon(t,\vec{\boldsymbol{x}}_q;\vec{\boldsymbol{x}}_s) = -\frac{1}{(2\pi)^3\varepsilon}\int T^\varepsilon_{\omega,\kappa}(-L,0)e^{-i\frac{\omega}{\varepsilon}(t-\boldsymbol{\kappa}\cdot(\boldsymbol{x}_q-\boldsymbol{x}_s)-L/c_0(\kappa))}\hat S(\omega,\boldsymbol{\kappa})\omega^2 d\omega d\boldsymbol{\kappa}\,, \quad (2.45)$$

$$\hat S(\omega,\boldsymbol{\kappa}) = \frac{1}{2}\Big[-\frac{\zeta_0(\kappa)}{\rho_0}\boldsymbol{\kappa}\cdot\hat{\boldsymbol{f}}_{\boldsymbol{x}}(\omega) + \hat f_z(\omega)\Big], \quad (2.46)$$

and the secondary field is

$$p_1^\varepsilon(t,\vec{\boldsymbol{x}}_q;\vec{\boldsymbol{x}}_s) = \frac{i\sigma_{\rm ref}}{2(2\pi)^5\varepsilon^2}\int\left(-\frac{\zeta_0(\kappa)\boldsymbol{\kappa}\cdot\boldsymbol{\kappa}'}{\rho_0} + \frac{\rho_0}{\zeta_0(\kappa')}\right)\hat S(\omega,\boldsymbol{\kappa})\omega^5 T^\varepsilon_{\omega,\kappa'}(-L,0) \times\Big[e^{i\frac{\omega}{\varepsilon}\phi_I(\boldsymbol{\kappa},\boldsymbol{\kappa}')} - \widetilde R^\varepsilon_{\omega,\kappa}(-L,0)e^{i\frac{\omega}{\varepsilon}\phi_{II}(\boldsymbol{\kappa},\boldsymbol{\kappa}')}\Big]d\omega d\boldsymbol{\kappa} d\boldsymbol{\kappa}'\,, \quad (2.47)$$

where the two rapidly varying phases are given by (2.31-2.32) again.

2.6. Cross Correlation of the Fields. In Subsection 2.6.2 we will give the asymptotic behavior of the cross correlation $\mathcal{C}^\varepsilon$ defined by (2.9) in the limit $\varepsilon \to 0$ and in the presence of a small reflector. We first give in Subsection 2.6.1 results concerning the moments of the transmission coefficients that are needed for our analysis.

2.6.1. The Statistics of the Transmission Coefficients. The first proposition gives the moments of the transmission coefficient [18, Chapter 7]. This is useful for computing the behavior of the coherent wave. The proposition shows that the mean transmission coefficient $T^\varepsilon_{\omega,\kappa}$ decays exponentially with the rate $\exp(-L/l_{\rm sca})$ where $l_{\rm sca} = 1/(\omega^2\gamma_\kappa)$ and γ_κ is defined by (2.50). The characteristic length $l_{\rm sca}$ is called the scattering mean free path in the physical literature.

PROPOSITION 2.3. *For any test function $\phi(\omega,\boldsymbol{\kappa})$, we have*

$$\int \phi(\omega,\boldsymbol{\kappa})T^\varepsilon_{\omega,\kappa}(-L,0)d\omega d\boldsymbol{\kappa} \stackrel{\varepsilon\to 0}{\longrightarrow} \int \phi(\omega,\boldsymbol{\kappa})T^{(0)}_{\omega,\kappa}(-L,0)d\omega d\boldsymbol{\kappa}, \quad (2.48)$$

$$T^{(0)}_{\omega,\kappa}(-L,0) = \exp\Big(i\omega\sqrt{\gamma_\kappa}W_0(L) - \frac{\omega^2\gamma_\kappa L}{2}\Big), \quad (2.49)$$

in distribution, where $W_0(L)$ is a standard Brownian motion and

$$\gamma_\kappa = \frac{\gamma c_0(\kappa)^2}{4c_0^4}. \tag{2.50}$$

The moments of the transmission coefficients are

$$\mathbb{E}\big[T^\varepsilon_{\omega,\kappa}(-L,0)^n\big] \stackrel{\varepsilon\to 0}{\longrightarrow} \exp\Big(-\frac{n^2+n}{2}\omega^2\gamma_\kappa L\Big). \tag{2.51}$$

The second proposition gives the moments of the power transmission coefficient [18, Chapter 7]. This is useful for computing the behavior of the incoherent waves. The proposition shows that the power transmission coefficient $|T^\varepsilon_{\omega,\kappa}|^2$ decays exponentially with the rate $\exp(-2L/l_{\rm loc})$ with $l_{\rm loc} = 8/(\omega^2\gamma_\kappa)$. The characteristic length $l_{\rm loc}$ is called the localization length in the physical literature. In a randomly layered medium the localization length and the scattering mean free path are proportional, but this is not true for other types of random media.

PROPOSITION 2.4. *The moments of the power transmission coefficients are*

$$\mathbb{E}\big[|T^\varepsilon_{\omega,\kappa}(-L,0)|^{2n}\big] \stackrel{\varepsilon\to 0}{\longrightarrow} \xi_n\big(\omega^2\gamma_\kappa L\big), \tag{2.52}$$

where

$$\xi_n(l) = \exp\Big(-\frac{l}{4}\Big)\int_0^\infty e^{-\mu^2 l}\frac{2\pi\mu\sinh(\pi\mu)}{\cosh^2(\pi\mu)}K^{(n)}(\mu)d\mu, \tag{2.53}$$

with $K^{(1)}(\mu) = 1$ and for $n \geq 2$:

$$K^{(n)}(\mu) = \prod_{j=1}^{n-1}\frac{1}{j^2}\Big[\mu^2 + \big(j-\frac{1}{2}\big)^2\Big].$$

The third proposition gives the first two moments (mean and variance) of the square modulus of the Green's function $|\mathcal{G}^\varepsilon_{\omega,\kappa}|^2$. This is useful for computing the behavior of the incoherent waves in the presence of pressure release boundary conditions.

PROPOSITION 2.5. *The mean of the square modulus of the Green's function is equal to one in the limit $\varepsilon \to 0$:*

$$\lim_{\varepsilon\to 0}\mathbb{E}\big[|\mathcal{G}^\varepsilon_{\omega,\kappa}|^2\big] = 1. \tag{2.54}$$

The variance of the square modulus of the Green's function has the limit:

$$\lim_{\varepsilon\to 0}\mathrm{Var}\big(|\mathcal{G}^\varepsilon_{\omega,\kappa}|^2\big) = \frac{6}{5}\exp\big(10\omega^2\gamma_\kappa L\big) - \frac{6}{5}. \tag{2.55}$$

These results were obtained in [24]. The proof is based on the expansion of the square modulus of the Green's function in a series expansion (from (2.20)) and in the evaluation of the expectation of each term of the expansion. It is important to understand that the relation (2.54) is true only after statistical averaging. The square modulus of the Green's function $|\mathcal{G}^\varepsilon_{\omega,\kappa}|^2$ has in fact large fluctuations when the medium is strongly random as shown by the expression of the variance.

We can briefly comment on the fact that $\mathbb{E}\big[|\mathcal{G}^\varepsilon_{\omega,\kappa}|^2\big] = 1$. When the medium is homogeneous it is straightforward to understand that the reflexion coefficient R^ε is

zero and the transmission coefficient T^ε is one so that the square modulus of the Green's function is equal to one. When the medium is strongly random, the reflexion coefficient of the random medium is close to one, so the wave is trapped within the waveguide formed by the deterministic surface at $z = 0$ and the random medium below it. The wave is reflected back and forth and the internal intensity within the random medium reaches high values. However, at the lower interface $z = -L$, it turns out that, on average, the intensity is one. In a heuristic sense, the wave has no other choice but to escape through the lower interface $z = -L$, but the transmitted wave is highly incoherent when the size L is larger than the localization length. This is a wave phenomenon that can be observed also in a purely deterministic situation, for instance in the presence of a strong interface at $z = -L$ instead of a random medium in $z \in (-L, 0)$. This case is addressed in Subsection 3.1 where we show that the square modulus of the Green's function has strong oscillations as a function of the frequency ω and the transverse wavenumber κ, but its average in frequency is one.

2.6.2. The Primary and Secondary Cross Correlations. The cross correlation $\mathcal{C}^\varepsilon$ of the signals recorded at the auxiliary array is defined by (2.9). In the presence of a reflector at $\vec{\boldsymbol{y}}$, it can be written as the sum

$$\mathcal{C}^\varepsilon(\tau, \vec{\boldsymbol{x}}_q, \vec{\boldsymbol{x}}_{q'}) = \mathcal{C}^\varepsilon_{\rm pp}(\tau, \vec{\boldsymbol{x}}_q, \vec{\boldsymbol{x}}_{q'}) + \mathcal{C}^\varepsilon_{\rm ps}(\tau, \vec{\boldsymbol{x}}_q, \vec{\boldsymbol{x}}_{q'}) + \mathcal{C}^\varepsilon_{\rm sp}(\tau, \vec{\boldsymbol{x}}_q, \vec{\boldsymbol{x}}_{q'}), \tag{2.56}$$

Here $\mathcal{C}^\varepsilon_{\rm pp}$ is the cross correlation of the primary field (2.27) at $\vec{\boldsymbol{x}}_q = (\boldsymbol{x}_q, -L)$ with the primary field at $\vec{\boldsymbol{x}}_{q'} = (\boldsymbol{x}_{q'}, -L)$,

$$\mathcal{C}^\varepsilon_{\rm pp}(\tau, \vec{\boldsymbol{x}}_q, \vec{\boldsymbol{x}}_{q'}) = \varepsilon^{-2} \int d\boldsymbol{x}_s \int dt p^\varepsilon_0(t, \vec{\boldsymbol{x}}_q; \vec{\boldsymbol{x}}_s) p^\varepsilon_0(t + \tau, \vec{\boldsymbol{x}}_{q'}; \vec{\boldsymbol{x}}_s), \tag{2.57}$$

$\mathcal{C}^\varepsilon_{\rm ps}$ is the cross correlation of the primary field (2.27) at $\vec{\boldsymbol{x}}_q$ with the secondary field (2.30) at $\vec{\boldsymbol{x}}_{q'}$,

$$\mathcal{C}^\varepsilon_{\rm ps}(\tau, \vec{\boldsymbol{x}}_q, \vec{\boldsymbol{x}}_{q'}) = \varepsilon^{-2} \int d\boldsymbol{x}_s \int dt p^\varepsilon_0(t, \vec{\boldsymbol{x}}_q; \vec{\boldsymbol{x}}_s) p^\varepsilon_1(t + \tau, \vec{\boldsymbol{x}}_{q'}; \vec{\boldsymbol{x}}_s), \tag{2.58}$$

and $\mathcal{C}^\varepsilon_{\rm sp}$ is the cross correlation of the secondary field (2.30) at $\vec{\boldsymbol{x}}_q$ with the primary field (2.27) at $\vec{\boldsymbol{x}}_{q'}$,

$$\mathcal{C}^\varepsilon_{\rm sp}(\tau, \vec{\boldsymbol{x}}_q, \vec{\boldsymbol{x}}_{q'}) = \varepsilon^{-2} \int d\boldsymbol{x}_s \int dt p^\varepsilon_1(t, \vec{\boldsymbol{x}}_q; \vec{\boldsymbol{x}}_s) p^\varepsilon_0(t + \tau, \vec{\boldsymbol{x}}_{q'}; \vec{\boldsymbol{x}}_s). \tag{2.59}$$

The next three propositions give the asymptotic behaviors of the primary cross correlation $\mathcal{C}^\varepsilon_{\rm pp}$ and of the secondary cross correlations $\mathcal{C}^\varepsilon_{\rm ps}$ and $\mathcal{C}^\varepsilon_{\rm sp}$. The convergence results hold true in distribution. When the limit is deterministic, then the convergence also holds true in probability.

PROPOSITION 2.6. *If* $\boldsymbol{x}_{q'} = \boldsymbol{x}_q + \varepsilon\boldsymbol{\xi}$ *and* $\tau = \varepsilon s$ *then*

$$\varepsilon \mathcal{C}^\varepsilon_{\rm pp}(\tau, \vec{\boldsymbol{x}}_q, \vec{\boldsymbol{x}}_{q'}) \stackrel{\varepsilon\to 0}{\longrightarrow} \delta(\boldsymbol{\xi}) \frac{1}{2\pi} \int |\hat{f}_z(\omega)|^2 e^{i\omega s} d\omega. \tag{2.60}$$

Moreover

$$\begin{aligned} &\frac{1}{\varepsilon} \int {\rm Var}\big(\mathcal{C}^\varepsilon_{\rm pp}(\tau, \vec{\boldsymbol{x}}_q, \vec{\boldsymbol{x}}_{q'})\big) d\tau d\boldsymbol{x}_{q'} \\ &\stackrel{\varepsilon\to 0}{\longrightarrow} \frac{6}{5(2\pi)^3} \int \Big[\exp\Big(\frac{5\gamma c_0(\kappa)^2 \omega^2 L}{2c_0^4} \Big) - 1 \Big] |\hat{f}_z(\omega)|^4 \omega^2 d\boldsymbol{\kappa} d\omega. \end{aligned} \tag{2.61}$$

The proposition shows that the primary cross correlation possesses a strong peak when $\boldsymbol{x}_{q'} \simeq \boldsymbol{x}_q$ centered at $\tau = 0$. Otherwise it has small fluctuations distributed in space and time lag that are of order $\varepsilon^{1/2}$.

Proof. We have

$$\mathcal{C}^\varepsilon(\vec{\boldsymbol{x}}_q, \vec{\boldsymbol{x}}_{q'}, \tau) = \frac{1}{(2\pi)^3 \varepsilon} \int |\mathcal{G}^\varepsilon_{\omega,\boldsymbol{\kappa}}|^2 e^{i\frac{\omega}{\varepsilon}(\boldsymbol{\kappa}\cdot(\boldsymbol{x}_q - \boldsymbol{x}_{q'}) + \tau)} |\hat{f}_z(\omega)|^2 \omega^2 d\boldsymbol{\kappa} d\omega.$$

Using the fact that $|\mathcal{G}^\varepsilon_{\omega,\boldsymbol{\kappa}}|^2$ is self-averaging and has mean one we obtain (2.60). The variance (2.60) follows from (2.55). □

PROPOSITION 2.7. *The ps-secondary cross correlation centered at $\tau = [|\vec{\boldsymbol{y}} - \vec{\boldsymbol{x}}_q| + |\vec{\boldsymbol{x}}_{q'} - \vec{\boldsymbol{y}}|]/c_0$ has the form:*

$$\begin{aligned}
&\mathcal{C}^\varepsilon_{\rm ps}\Big(\frac{|\vec{\boldsymbol{y}} - \vec{\boldsymbol{x}}_q| + |\vec{\boldsymbol{x}}_{q'} - \vec{\boldsymbol{y}}|}{c_0} + \varepsilon s, \vec{\boldsymbol{x}}_q, \vec{\boldsymbol{x}}_{q'}\Big) \\
&\stackrel{\varepsilon\to 0}{\longrightarrow} \frac{i\sigma_{\rm ref}}{2(2\pi)^3 c_0^3} \frac{|L_y - L|\,(\vec{\boldsymbol{y}} - \vec{\boldsymbol{x}}_q)\cdot(\vec{\boldsymbol{x}}_{q'} - \vec{\boldsymbol{y}})}{|\vec{\boldsymbol{y}} - \vec{\boldsymbol{x}}_q|^3\,|\vec{\boldsymbol{x}}_{q'} - \vec{\boldsymbol{y}}|^2} \int |\hat{f}_z(\omega)|^2 \omega^3 \exp\big(i\omega s\big) d\omega. \qquad (2.62)
\end{aligned}$$

The ps-secondary cross correlation centered at $\tau = [|\vec{\boldsymbol{y}} - \vec{\boldsymbol{x}}_q| + |\vec{\boldsymbol{x}}^{(\rm s)}_{q'} - \vec{\boldsymbol{y}}|]/c_0$ has the form:

$$\begin{aligned}
&\mathcal{C}^\varepsilon_{\rm ps}\Big(\frac{|\vec{\boldsymbol{y}} - \vec{\boldsymbol{x}}_q| + |\vec{\boldsymbol{x}}^{(\rm s)}_{q'} - \vec{\boldsymbol{y}}|}{c_0} + \varepsilon s, \vec{\boldsymbol{x}}_q, \vec{\boldsymbol{x}}_{q'}\Big) \\
&\stackrel{\varepsilon\to 0}{\longrightarrow} -\frac{i\sigma_{\rm ref}}{2(2\pi)^3 c_0^3} \frac{|L + L_y|\,(\vec{\boldsymbol{y}} - \vec{\boldsymbol{x}}_q)\cdot(\vec{\boldsymbol{x}}^{(\rm s)}_{q'} - \vec{\boldsymbol{y}})}{|\vec{\boldsymbol{y}} - \vec{\boldsymbol{x}}_q|^3\,|\vec{\boldsymbol{x}}^{(\rm s)}_{q'} - \vec{\boldsymbol{y}}|^2} \\
&\qquad \times \int |\hat{f}_z(\omega)|^2 \omega^3 \exp\Big(i\omega\big(s - 2\sqrt{\gamma_{\boldsymbol{x}^{(\rm s)}_{q'}}} W_0(L)\big) - \omega^2 \gamma_{\boldsymbol{x}^{(\rm s)}_{q'}} L\Big) d\omega, \qquad (2.63)
\end{aligned}$$

where $\vec{\boldsymbol{x}}^{(\rm s)}_{q'} = (\boldsymbol{x}_{q'}, L)$ is the point obtained from $\vec{\boldsymbol{x}}_{q'} = (\boldsymbol{x}_{q'}, -L)$ by a symmetry with respect to the surface $z = 0$ and

$$\gamma_{\boldsymbol{x}^{(\rm s)}_{q'}} = \frac{\gamma}{4c_0^2} \frac{|\vec{\boldsymbol{x}}^{(\rm s)}_{q'} - \vec{\boldsymbol{y}}|^2}{(L + L_y)^2}.$$

The ps-secondary cross correlation is negligible elsewhere.

Proof. After integration in t an $\boldsymbol{x}_s$, the expression of the *ps*-secondary cross correlation is

$$\begin{aligned}
\mathcal{C}^\varepsilon_{\rm ps}(\tau, \vec{\boldsymbol{x}}_q, \vec{\boldsymbol{x}}_{q'}) &= \frac{i\sigma_{\rm ref}}{2(2\pi)^5 \varepsilon^2} \int |\hat{f}_z(\omega)|^2 \big(-\frac{\zeta_0(\kappa')}{\rho_0} \boldsymbol{\kappa}' \cdot \boldsymbol{\kappa} + \frac{\rho_0}{\zeta_0(\kappa)}\big) \big|\mathcal{G}^\varepsilon_{\omega,\boldsymbol{\kappa}}\big|^2 \\
&\quad \times \Big(e^{i\frac{\omega}{\varepsilon}\psi_I(\boldsymbol{\kappa},\boldsymbol{\kappa}')} - \big(\overline{\widetilde{R}^\varepsilon_{\omega,\kappa'}}(-L,0) + \frac{\overline{T^\varepsilon_{\omega,\kappa'}}^2}{1 - \overline{T^\varepsilon_{\omega,\kappa'}}}(-L,0)\big) e^{i\frac{\omega}{\varepsilon}\psi_{II}(\boldsymbol{\kappa},\boldsymbol{\kappa}')}\Big) \omega^5 d\boldsymbol{\kappa} d\boldsymbol{\kappa}' d\omega, \\
\psi_I(\boldsymbol{\kappa},\boldsymbol{\kappa}') &= \boldsymbol{\kappa}\cdot(\boldsymbol{x}_q - \boldsymbol{y}) + \frac{L - L_y}{c_0(\kappa)} - \boldsymbol{\kappa}'\cdot(\boldsymbol{x}_{q'} - \boldsymbol{y}) + \frac{L - L_y}{c_0(\kappa')} + \tau, \\
\psi_{II}(\boldsymbol{\kappa},\boldsymbol{\kappa}') &= \boldsymbol{\kappa}\cdot(\boldsymbol{x}_q - \boldsymbol{y}) + \frac{L - L_y}{c_0(\kappa)} - \boldsymbol{\kappa}'\cdot(\boldsymbol{x}_{q'} - \boldsymbol{y}) + \frac{-L - L_y}{c_0(\kappa')} + \tau.
\end{aligned}$$

We then apply the stationary phase method. We find that the stationary points for the terms with the rapid phases ψ_I and ψ_{II} are respectively:

$$\boldsymbol{\kappa}_{\mathrm{sp},I} = \frac{1}{c_0}\frac{\boldsymbol{y}-\boldsymbol{x}_q}{\sqrt{|\boldsymbol{y}-\boldsymbol{x}_q|^2+(L-L_y)^2}}, \qquad \boldsymbol{\kappa}'_{\mathrm{sp},I} = \frac{1}{c_0}\frac{\boldsymbol{x}_{q'}-\boldsymbol{y}}{\sqrt{|\boldsymbol{x}_{q'}-\boldsymbol{y}|^2+(L-L_y)^2}},$$

and

$$\boldsymbol{\kappa}_{\mathrm{sp},II} = \frac{1}{c_0}\frac{\boldsymbol{y}-\boldsymbol{x}_q}{\sqrt{|\boldsymbol{y}-\boldsymbol{x}_q|^2+(L-L_y)^2}}, \qquad \boldsymbol{\kappa}'_{\mathrm{sp},II} = \frac{1}{c_0}\frac{\boldsymbol{x}_{q'}-\boldsymbol{y}}{\sqrt{|\boldsymbol{x}_{q'}-\boldsymbol{y}|^2+(L+L_y)^2}},$$

that give the first and second peak described in the proposition. □

PROPOSITION 2.8. *The sp-secondary cross correlation centered at* $\tau = -[|\vec{\boldsymbol{y}}-\vec{\boldsymbol{x}}_q|+|\vec{\boldsymbol{x}}_{q'}-\vec{\boldsymbol{y}}|]/c_0$ *has the form:*

$$\begin{aligned}&\mathcal{C}^{\varepsilon}_{\mathrm{sp}}\Big(-\frac{|\vec{\boldsymbol{y}}-\vec{\boldsymbol{x}}_q|+|\vec{\boldsymbol{x}}_{q'}-\vec{\boldsymbol{y}}|}{c_0}+\varepsilon s,\vec{\boldsymbol{x}}_q,\vec{\boldsymbol{x}}_{q'}\Big)\\ &\xrightarrow{\varepsilon\to 0}\frac{i\sigma_{\mathrm{ref}}}{2(2\pi)^3c_0^3}\frac{|L_y-L|\,(\vec{\boldsymbol{y}}-\vec{\boldsymbol{x}}_q)\cdot(\vec{\boldsymbol{x}}_{q'}-\vec{\boldsymbol{y}})}{|\vec{\boldsymbol{y}}-\vec{\boldsymbol{x}}_q|^2\,|\vec{\boldsymbol{x}}_{q'}-\vec{\boldsymbol{y}}|^3}\int|\hat{f}_z(\omega)|^2\omega^3\exp\big(-i\omega s\big)d\omega. \qquad (2.64)\end{aligned}$$

The sp-secondary cross correlation centered at $\tau = -[|\vec{\boldsymbol{y}}-\vec{\boldsymbol{x}}_q^{(\mathrm{s})}|+|\vec{\boldsymbol{x}}_{q'}-\vec{\boldsymbol{y}}|]/c_0$ *has the form:*

$$\begin{aligned}&\mathcal{C}^{\varepsilon}_{\mathrm{sp}}\Big(-\frac{|\vec{\boldsymbol{y}}-\vec{\boldsymbol{x}}_q^{(\mathrm{s})}|+|\vec{\boldsymbol{x}}_{q'}-\vec{\boldsymbol{y}}|}{c_0}+\varepsilon s,\vec{\boldsymbol{x}}_q,\vec{\boldsymbol{x}}_{q'}\Big)\\ &\xrightarrow{\varepsilon\to 0}\frac{i\sigma_{\mathrm{ref}}}{2(2\pi)^3c_0^3}\frac{|L_y-L|\,(\vec{\boldsymbol{y}}-\vec{\boldsymbol{x}}_q^{(\mathrm{s})})\cdot(\vec{\boldsymbol{x}}_{q'}-\vec{\boldsymbol{y}})}{|\vec{\boldsymbol{y}}-\vec{\boldsymbol{x}}_q^{(\mathrm{s})}|^2\,|\vec{\boldsymbol{x}}_{q'}-\vec{\boldsymbol{y}}|^3}\\ &\qquad\times\int|\hat{f}_z(\omega)|^2\omega^3\exp\Big(i\omega\big(-s-2\sqrt{\gamma_{\boldsymbol{x}_q^{(\mathrm{s})}}}W_0(L)\big)-\omega^2\gamma_{\boldsymbol{x}_q^{(\mathrm{s})}}L\Big)d\omega, \qquad (2.65)\end{aligned}$$

where $\vec{\boldsymbol{x}}_q^{(\mathrm{s})} = (\boldsymbol{x}_q, L)$ *is the point obtained from* $\vec{\boldsymbol{x}}_q = (\boldsymbol{x}_q, -L)$ *by a symmetry with respect to the surface* $z = 0$ *and*

$$\gamma_{\boldsymbol{x}_q^{(\mathrm{s})}} = \frac{\gamma}{4c_0^2}\frac{|\vec{\boldsymbol{y}}-\vec{\boldsymbol{x}}_q^{(\mathrm{s})}|^2}{(L+L_y)^2}.$$

The sp-secondary cross correlation is negligible elsewhere.

Note that $\tau \to (\mathcal{C}^{\varepsilon}_{\mathrm{ps}}+\mathcal{C}^{\varepsilon}_{\mathrm{sp}})(\tau,\vec{\boldsymbol{x}}_q,\vec{\boldsymbol{x}}_{q'})$ is close to be an even function, but not exactly. It has two quasi-symmetric peaks at $\pm[|\vec{\boldsymbol{y}}-\vec{\boldsymbol{x}}_q|+|\vec{\boldsymbol{x}}_{q'}-\vec{\boldsymbol{y}}|]/c_0$, which are approximations of the causal and anti-causal Green's function from $\vec{\boldsymbol{x}}_q$ to $\vec{\boldsymbol{x}}_{q'}$ through a scattering event at $\vec{\boldsymbol{y}}$. The phases of the cross correlation and of the Green's function coincide exactly, but the amplitudes are not equal because the illumination of the auxiliary receiver array is not uniform and isotropic, so that the Helmholtz-Kirchhoff identity that usually ensures the equivalence between cross correlations and Green's functions cannot be applied [21].

2.6.3. Separation between Up- and Down-Going Waves. As shown in the previous subsection, there are small fluctuations and additional peaks in the cross correlation that may affect the quality of the image. It is possible to remove these fluctuations and additional peaks if the three-dimensional velocity components are recorded (the vertical velocity field and the pressure field would be an alternative).

Indeed, if the three-dimensional velocity field is recorded at the receiver array at depth $z = -L$, then by taking a Fourier transform in time and lateral spatial variables (defined by (A.1-A.2)) it is possible to compute the up-going field:

$$\hat{p}^\varepsilon_{\rm u}(\omega,(\boldsymbol{\kappa},-L);\vec{\boldsymbol{x}}_s) = \frac{\zeta_0(\kappa)}{2}\hat{u}^\varepsilon(\omega,(\boldsymbol{\kappa},-L);\vec{\boldsymbol{x}}_s) + \frac{\rho_0\boldsymbol{\kappa}}{2\kappa^2}\cdot\hat{\boldsymbol{v}}^\varepsilon(\omega,(\boldsymbol{\kappa},-L);\vec{\boldsymbol{x}}_s) \tag{2.66}$$

and the down-going field:

$$\hat{p}^\varepsilon_{\rm d}(\omega,(\boldsymbol{\kappa},-L);\vec{\boldsymbol{x}}_s) = -\frac{\zeta_0(\kappa)}{2}\hat{u}^\varepsilon(\omega,(\boldsymbol{\kappa},-L);\vec{\boldsymbol{x}}_s) + \frac{\rho_0\boldsymbol{\kappa}}{2\kappa^2}\cdot\hat{\boldsymbol{v}}^\varepsilon(\omega,(\boldsymbol{\kappa},-L);\vec{\boldsymbol{x}}_s). \tag{2.67}$$

The up-going primary and secondary fields at the auxiliary array $\vec{\boldsymbol{x}}_q = (\boldsymbol{x}_q,-L)$ are

$$p^\varepsilon_{\rm u,0}(t,\vec{\boldsymbol{x}}_q;\vec{\boldsymbol{x}}_s) = 0, \tag{2.68}$$

$$p^\varepsilon_{\rm u,1}(t,\vec{\boldsymbol{x}}_q;\vec{\boldsymbol{x}}_s) = \frac{1}{(2\pi)^3\varepsilon}\int\frac{\sqrt{\zeta_0(\kappa)}}{2}\hat{a}^\varepsilon_1(\omega,\boldsymbol{\kappa},-L)e^{-i\frac{\omega}{\varepsilon}(t-\boldsymbol{\kappa}\cdot(\boldsymbol{x}_q-\boldsymbol{x}_s)+L/c_0(\kappa))}\omega^2 d\boldsymbol{\kappa}d\omega, \tag{2.69}$$

where $\hat{a}^\varepsilon_1$ is given by (2.43). The down-going primary and secondary fields at the auxiliary array are

$$p^\varepsilon_{\rm d,0}(t,\vec{\boldsymbol{x}}_q;\vec{\boldsymbol{x}}_s) = \frac{-1}{(2\pi)^3\varepsilon}\int\mathcal{G}^\varepsilon_{\omega,\kappa}\hat{f}_z(\omega)e^{-i\frac{\omega}{\varepsilon}(t-\boldsymbol{\kappa}\cdot(\boldsymbol{x}_q-\boldsymbol{x}_s)-L/c_0(\kappa))}\omega^2 d\boldsymbol{\kappa}d\omega, \tag{2.70}$$

$$p^\varepsilon_{\rm d,1}(t,\vec{\boldsymbol{x}}_q;\vec{\boldsymbol{x}}_s) = \frac{-1}{(2\pi)^3\varepsilon}\int\frac{\sqrt{\zeta_0(\kappa)}}{2}\hat{b}^\varepsilon_1(\omega,\boldsymbol{\kappa},-L)e^{-i\frac{\omega}{\varepsilon}(t-\boldsymbol{\kappa}\cdot(\boldsymbol{x}_q-\boldsymbol{x}_s)-L/c_0(\kappa))}\omega^2 d\boldsymbol{\kappa}d\omega, \tag{2.71}$$

where $\hat{b}^\varepsilon_1$ is given by (2.44). As a consequence, the cross correlation of the down-going field with the up-going field completely eliminates the contribution of the primary cross correlation, and the secondary cross correlation reduces to the cross correlation of $p^\varepsilon_{\rm u,1}$ with $p^\varepsilon_{\rm d,0}$, which eliminates the additional components present in $p^\varepsilon_{\rm d,1}$. We obtain the following proposition.

PROPOSITION 2.9. *Let us define*

$$\mathcal{C}^{\varepsilon,{\rm du}}(\tau,\vec{\boldsymbol{x}}_q,\vec{\boldsymbol{x}}_{q'}) = \varepsilon^{-2}\int d\boldsymbol{x}_s\int dt p^\varepsilon_{\rm d}(t,\vec{\boldsymbol{x}}_q;\vec{\boldsymbol{x}}_s)p^\varepsilon_{\rm u}(t+\tau,\vec{\boldsymbol{x}}_{q'};\vec{\boldsymbol{x}}_s). \tag{2.72}$$

As $\varepsilon\to 0$, there is no term of order one in $\sigma_{\rm ref}$, and the term of order $\sigma_{\rm ref}$ has only one peak centered at $\tau = [|\vec{\boldsymbol{y}}-\vec{\boldsymbol{x}}_q| + |\vec{\boldsymbol{x}}_{q'}-\vec{\boldsymbol{y}}|]/c_0$:

$$\begin{aligned}&\mathcal{C}^{\varepsilon,{\rm du}}\Big(\frac{|\vec{\boldsymbol{y}}-\vec{\boldsymbol{x}}_q|+|\vec{\boldsymbol{x}}_{q'}-\vec{\boldsymbol{y}}|}{c_0}+\varepsilon s,\vec{\boldsymbol{x}}_q,\vec{\boldsymbol{x}}_{q'}\Big)\\ &\stackrel{\varepsilon\to 0}{\longrightarrow}\frac{i\sigma_{\rm ref}}{2(2\pi)^3c_0^3}\frac{|L_y-L|\,(\vec{\boldsymbol{y}}-\vec{\boldsymbol{x}}_q)\cdot(\vec{\boldsymbol{x}}_{q'}-\vec{\boldsymbol{y}})}{|\vec{\boldsymbol{y}}-\vec{\boldsymbol{x}}_q|^3\,|\vec{\boldsymbol{x}}_{q'}-\vec{\boldsymbol{y}}|^2}\int|\hat{f}_z(\omega)|^2\omega^3\exp\big(i\omega s\big)d\omega.\end{aligned} \tag{2.73}$$

Let us define

$$\mathcal{C}^{\varepsilon,{\rm ud}}(\tau,\vec{\boldsymbol{x}}_q,\vec{\boldsymbol{x}}_{q'}) = \varepsilon^{-2}\int d\boldsymbol{x}_s\int dt p^\varepsilon_{\rm u}(t,\vec{\boldsymbol{x}}_q)p^\varepsilon_{\rm d}(t+\tau,\vec{\boldsymbol{x}}_{q'}). \tag{2.74}$$

As $\varepsilon\to 0$, there is no term of order one in $\sigma_{\rm ref}$, and the term of order $\sigma_{\rm ref}$ has only one peak centered at $\tau = -[|\vec{\boldsymbol{y}}-\vec{\boldsymbol{x}}_q| + |\vec{\boldsymbol{x}}_{q'}-\vec{\boldsymbol{y}}|]/c_0$:

$$\begin{aligned}&\mathcal{C}^{\varepsilon,{\rm ud}}\Big(-\frac{|\vec{\boldsymbol{y}}-\vec{\boldsymbol{x}}_q|+|\vec{\boldsymbol{x}}_{q'}-\vec{\boldsymbol{y}}|}{c_0}+\varepsilon s,\vec{\boldsymbol{x}}_q,\vec{\boldsymbol{x}}_{q'}\Big)\\ &\stackrel{\varepsilon\to 0}{\longrightarrow}\frac{i\sigma_{\rm ref}}{2(2\pi)^3c_0^3}\frac{|L_y-L|\,(\vec{\boldsymbol{y}}-\vec{\boldsymbol{x}}_q)\cdot(\vec{\boldsymbol{x}}_{q'}-\vec{\boldsymbol{y}})}{|\vec{\boldsymbol{y}}-\vec{\boldsymbol{x}}_q|^2\,|\vec{\boldsymbol{x}}_{q'}-\vec{\boldsymbol{y}}|^3}\int|\hat{f}_z(\omega)|^2\omega^3\exp\big(-i\omega s\big)d\omega.\end{aligned} \tag{2.75}$$

In order to exploit all the data set, one can therefore form the sum:

$$\mathcal{C}^{\varepsilon}(\vec{\boldsymbol{x}}_q, \vec{\boldsymbol{x}}_{q'}, \tau) = \frac{1}{2}\big[\mathcal{C}^{\varepsilon,\mathrm{du}}(\vec{\boldsymbol{x}}_q, \vec{\boldsymbol{x}}_{q'}, \tau) + \mathcal{C}^{\varepsilon,\mathrm{ud}}(\vec{\boldsymbol{x}}_q, \vec{\boldsymbol{x}}_{q'}, -\tau)\big] \tag{2.76}$$

that possesses a peak with higher amplitude centered at $\tau = [|\vec{\boldsymbol{y}} - \vec{\boldsymbol{x}}_q| + |\vec{\boldsymbol{x}}_{q'} - \vec{\boldsymbol{y}}|]/c_0$.

2.7. Detailed Analysis of Kirchhoff Migration.

2.7.1. Migration of the Cross Correlation Matrix. In this section we study the migration of the cross correlation matrix. We use the cross correlation of the up-going and down-going field (2.76) if the three-dimensional velocity field has been recorded, or the cross correlation of the pressure field with itself if only the pressure field is recorded. In the first case the cross correlation only presents a peak at (plus and minus) the sum of travel times $[|\vec{\boldsymbol{x}}_q - \vec{\boldsymbol{y}}| + |\vec{\boldsymbol{y}} - \vec{\boldsymbol{x}}_{q'}|]/c_0$ which is perfect for imaging. In the second case the cross correlation also presents peaks at (plus or minus) the sums of travel times $[|\vec{\boldsymbol{x}}_q - \vec{\boldsymbol{y}}| + |-\vec{\boldsymbol{y}} - \vec{\boldsymbol{x}}^{(\mathrm{s})}_{q'}|]/c_0$ and $[|\vec{\boldsymbol{x}}^{(\mathrm{s})}_q - \vec{\boldsymbol{y}}| + |\vec{\boldsymbol{y}} - \vec{\boldsymbol{x}}_{q'}|]/c_0$. These peaks are randomly shifted and they are exponentially damped as shown by Propositions 2.7-2.8. As a consequence, if the up- and down-going waves decomposition is not available, then strong scattering by the random medium is in fact favorable as it cancels the additional peaks.

The Kirchhoff migration function for the search point $\vec{\boldsymbol{y}}^S$ is

$$\mathcal{I}^{\varepsilon}_{\mathrm{C}}(\vec{\boldsymbol{y}}^S) = \frac{1}{N_{\mathrm{q}}^2}\sum_{q,q'=1}^{N_{\mathrm{q}}} \mathcal{C}^{\varepsilon}\Big(\frac{|\vec{\boldsymbol{x}}_q - \vec{\boldsymbol{y}}^S| + |\vec{\boldsymbol{y}}^S - \vec{\boldsymbol{x}}_{q'}|}{c_0}, \vec{\boldsymbol{x}}_q, \vec{\boldsymbol{x}}_{q'}\Big), \tag{2.77}$$

where N_{q} is the number of receivers at the auxiliary array.

If the receiver array at depth $-L$ is a dense square array centered at $\boldsymbol{x}_A$ and with sidelength a, so that we can replace the discrete sums by continuous integrals:

$$\frac{1}{N_{\mathrm{q}}^2}\sum_{q,q'=1}^{N_{\mathrm{q}}} \approx \frac{1}{a^4}\int_{\boldsymbol{x}_q - \boldsymbol{x}_A \in [-a/2,a/2]^2} d\boldsymbol{x}_q \int_{\boldsymbol{x}_{q'} - \boldsymbol{x}_A \in [-a/2,a/2]^2} d\boldsymbol{x}_{q'},$$

then, denoting the search point by

$$\vec{\boldsymbol{y}}^S = \vec{\boldsymbol{y}} + (\boldsymbol{\xi}, \eta), \tag{2.78}$$

we have

$$\begin{aligned}\mathcal{I}^{\varepsilon}_{\mathrm{C}}(\vec{\boldsymbol{y}}^S) \overset{\varepsilon\to 0}{\longrightarrow} \frac{i\sigma_{\mathrm{ref}}}{2(2\pi)^3 c_0^3 (L_y - L)^2}\int \omega^3 |\hat{f}_z(\omega)|^2 \exp\Big(2i\frac{\omega}{c_0}(\eta + \boldsymbol{\xi}\cdot\frac{\boldsymbol{x}_A - \boldsymbol{y}}{L_y - L})\Big) \\ \times \mathrm{sinc}^2\Big(\frac{a\xi_1\omega}{2c_0(L_y - L)}\Big)\mathrm{sinc}^2\Big(\frac{a\xi_2\omega}{2c_0(L_y - L)}\Big)d\omega.\end{aligned} \tag{2.79}$$

In order to simplify the expression we have assumed that the sidelength a is smaller than the depth $L_y - L$. If, in addition, the bandwidth B of the probing pulse is small compared to the central frequency ω_0, then we have (2.11).

2.7.2. Migration of the Surface Array Data. The data set is here the signals (vertical velocity fields) recorded at the surface $z = 0$ at points $\vec{\boldsymbol{x}}_r = (\boldsymbol{x}_r, 0)$ and emitted by a point source at $\vec{\boldsymbol{x}}_s = (\boldsymbol{x}_s, 0)$. The Kirchhoff migration function for the search point $\vec{\boldsymbol{y}}^S$ is

$$\mathcal{I}^\varepsilon_{\rm S}(\vec{\boldsymbol{y}}^S) = \frac{1}{N_{\rm s}N_{\rm r}} \sum_{s=1}^{N_{\rm s}} \sum_{r=1}^{N_{\rm r}} u^\varepsilon\Big(\frac{|\vec{\boldsymbol{x}}_s - \vec{\boldsymbol{y}}^S| + |\vec{\boldsymbol{y}}^S - \vec{\boldsymbol{x}}_r|}{c_0}, \vec{\boldsymbol{x}}_r; \vec{\boldsymbol{x}}_s\Big), \tag{2.80}$$

where $N_{\rm s}$ is the number of sources and $N_{\rm r}$ is the number of observation points at the surface. In the following we analyze two situations: in the first one *(I)* the surface array is finite; in the second one *(II)* the surface array is infinite.

(I) If the source and receiver array at the surface $z = 0$ are a dense square array centered at $\boldsymbol{x}_A$ and with sidelength a, then, denoting the search point by (2.78), we have

$$\begin{aligned}\mathcal{I}^\varepsilon_{\rm S}(\vec{\boldsymbol{y}}^S) \stackrel{\varepsilon\to 0}{\longrightarrow} \frac{i\sigma_{\rm ref}}{2(2\pi)^3 L_y^2} \int \omega^3 \hat{f}_z(\omega) \exp\Big(2i\frac{\omega}{c_0}(\eta + \boldsymbol{\xi}\cdot\frac{\boldsymbol{x}_A - \boldsymbol{y}}{L_y})\Big) \\ \times \mathrm{sinc}^2\Big(\frac{a\xi_1\omega}{2c_0L_y}\Big)\mathrm{sinc}^2\Big(\frac{a\xi_2\omega}{2c_0L_y}\Big) \exp\Big(i\omega\frac{\sqrt{\gamma}}{\sqrt{2}c_0}W_0(L) - \frac{\gamma\omega^2}{4c_0^2}L\Big)d\omega. \end{aligned} \tag{2.81}$$

In order to simplify the expression we have here assumed that the sidelength a is smaller than the depth L_y. If, in addition, the bandwidth B of the probing pulse is small compared to the central frequency ω_0, then we have (2.16).

(II) If the source and receiver array at the surface $z = 0$ are a dense array that covers completely the surface, then we have

$$\begin{aligned}\mathcal{I}^\varepsilon_{\rm S}(\vec{\boldsymbol{y}}^S) \stackrel{\varepsilon\to 0}{\longrightarrow} \frac{i\sigma_{\rm ref}L_y^2}{2(2\pi)} \int \omega^3 \hat{f}_z(\omega) \exp\Big(2i\frac{\omega}{c_0}\eta + i\omega\frac{\sqrt{\gamma}}{\sqrt{2}c_0}W_0(L) - \frac{\gamma\omega^2}{4c_0^2}L\Big) \\ \times\Big(\frac{\gamma\omega^2}{4c_0^2}L - i\omega\frac{\sqrt{\gamma}}{2\sqrt{2}c_0}W_0(L)\Big)^{-2} \exp\Big[-\frac{\omega^2|\boldsymbol{\xi}|^2}{c_0^2\big(\frac{\gamma\omega^2}{4c_0^2}L - i\omega\frac{\sqrt{\gamma}}{2\sqrt{2}c_0}W_0(L)\big)}\Big]d\omega \end{aligned} \tag{2.82}$$

Here we have assumed that the damping due to the random fluctuations is strong $\omega_0^2\gamma L/c_0^2 > 1$. If, in addition, the bandwidth B of the probing pulse is small compared to the central frequency ω_0, then we have (2.14).

2.7.3. Migration of the Auxiliary Array Data. The data set is here the signals (pressure fields or vertical velocity fields) recorded at the auxiliary passive array at points $\vec{\boldsymbol{x}}_q = (\boldsymbol{x}_q, -L)$ and emitted by a point source at $\vec{\boldsymbol{x}}_s = (\boldsymbol{x}_s, 0)$. This is exactly the same data set as the one used in the function (2.10). The Kirchhoff migration function for the search point $\vec{\boldsymbol{y}}^S$ is

$$\mathcal{I}^\varepsilon_{\rm R}(\vec{\boldsymbol{y}}^S) = \frac{1}{N_{\rm s}N_{\rm q}} \sum_{s=1}^{N_{\rm s}} \sum_{q=1}^{N_{\rm q}} p^\varepsilon\Big(\frac{|\vec{\boldsymbol{x}}_s - \vec{\boldsymbol{y}}^S| + |\vec{\boldsymbol{y}}^S - \vec{\boldsymbol{x}}_q|}{c_0}, \vec{\boldsymbol{x}}_q; \vec{\boldsymbol{x}}_s\Big), \tag{2.83}$$

where $N_{\rm s}$ is the number of sources at the surface and $N_{\rm q}$ is the number of receivers in the auxiliary passive array. The recorded field p^ε is the sum of the primary field p_0^ε given by (2.27) and of the secondary field p_1^ε given by (2.30), which contains the information about the reflector at $\vec{\boldsymbol{y}}$. If it is possible, the decomposition of the recorded field into up-going and down-going waves can be useful to reduce the noise level: by migrating only the up-going wave, only the first component in p_1^ε in (2.30) is migrated.

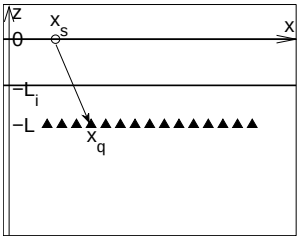

FIG. 3.1. *Emission from a point source located at* $\vec{\boldsymbol{x}}_s = (\boldsymbol{x}_s, 0)$. *The receiver is located at depth* $-L$: $\vec{\boldsymbol{x}}_q = (\boldsymbol{x}_q, -L)$. *There is an interface at depth* $z = -L_{\rm i}$.

If the source array at the surface $z = 0$ is a dense array that covers completely the surface and if the auxiliary receiver array is a dense square array centered at $\boldsymbol{x}_A$ and with sidelength a, then, denoting the search point by (2.78), we have

$$\mathcal{I}^{\varepsilon}_{\rm R}(\vec{\boldsymbol{y}}^S) \stackrel{\varepsilon\to 0}{\longrightarrow} -\frac{i\sigma_{\rm ref} L_y}{2(2\pi)^2(L_y-L)} \int \omega^3 \hat{f}_z(\omega) \exp\Big(i\frac{\omega}{c_0}\big(2\eta + \boldsymbol{\xi}\cdot\frac{\boldsymbol{x}_A-\boldsymbol{y}}{L_y-L}\big)\Big)$$
$$\times \mathrm{sinc}\Big(\frac{a\xi_1\omega}{2c_0(L_y-L)}\Big)\mathrm{sinc}\Big(\frac{a\xi_2\omega}{2c_0(L_y-L)}\Big) \exp\Big(i\omega\frac{\sqrt{\gamma}}{2c_0}W_0(L) - \frac{\gamma\omega^2}{8c_0^2}L\Big)$$
$$\times\Big(\frac{\gamma\omega^2}{4c_0^2}L - i\omega\frac{\sqrt{\gamma}}{2c_0}W_0(L)\Big)^{-1} \exp\Big[-\frac{\omega^2|\boldsymbol{\xi}|^2}{c_0^2\big(\frac{\gamma\omega^2}{2c_0^2}L - i\omega\frac{\sqrt{\gamma}}{c_0}W_0(L)\big)}\Big] d\omega. \qquad (2.84)$$

In order to simplify the expression we have here assumed that the sidelength a is smaller than the depth L_y and we have assumed that the damping due to the random fluctuations is strong $\omega_0^2\gamma L/c_0^2 > 1$. If, in addition, the bandwidth B of the probing pulse is small compared to the central frequency ω_0, then we have (2.16).

3. Imaging through a Strong Interface. In this section we depart from the situation with a homogeneous background medium modulated by random fluctuations, which is our main focus, and discuss the case of a background medium with a strong and deterministic interface and without random fluctuations. This allows us to contrast the wave multiples seen in a random medium with the ones obtained in a homogeneous medium and generated by a jump in the background. In Section 3.1 we describe the primary field (the field without the embedded reflector). In Section 3.2 we describe the secondary field (the field scattered by the embedded reflector in the Born approximation). In Sections 3.3-3.4 we analyze the migration of the cross correlations of the auxiliary array data.

3.1. Primary Field. We assume that the density and bulk modulus of the medium are stepwise constant (see Figure 3.1):

$$K^{\varepsilon\,-1}(z) = \begin{cases} K_1^{-1} & \text{if } z \in (-\infty, -L_{\rm i}) \\ K_0^{-1} & \text{if } z \in (-L_{\rm i}, 0) \end{cases}, \qquad (3.1)$$

$$\rho^{\varepsilon}(z) = \begin{cases} \rho_1 & \text{if } z \in (-\infty, -L_{\rm i}) \\ \rho_0 & \text{if } z \in (-L_{\rm i}, 0) \end{cases}, \qquad (3.2)$$

giving a jump in the impedance at the interface $z = -L_{\rm i}$, where $-L_{\rm i} \in (-L, 0)$. The pressure field at the surface $z = 0$ is zero. In these conditions we find by the

method of Appendix A that the pressure and vertical velocity fields recorded at a point $\vec{\boldsymbol{x}} = (\boldsymbol{x}, z)$ at depth $z \leq -L$ have the representations:

$$u^\varepsilon(t,\vec{\boldsymbol{x}};\vec{\boldsymbol{x}}_s) = \frac{1}{(2\pi)^3\varepsilon}\int \mathcal{G}^\varepsilon_{\omega,\kappa}\frac{\hat{f}_z(\omega)}{\sqrt{\zeta_0(\kappa)\zeta_1(\kappa)}}e^{-i\frac{\omega}{\varepsilon}(t-\boldsymbol{\kappa}\cdot(\boldsymbol{x}-\boldsymbol{x}_s)+z/c_1(\kappa))}\omega^2 d\boldsymbol{\kappa}d\omega, \quad (3.3)$$

$$p^\varepsilon(t,\vec{\boldsymbol{x}};\vec{\boldsymbol{x}}_s) = -\frac{1}{(2\pi)^3\varepsilon}\int \mathcal{G}^\varepsilon_{\omega,\kappa}\frac{\sqrt{\zeta_1(\kappa)}}{\sqrt{\zeta_0(\kappa)}}\hat{f}_z(\omega)e^{-i\frac{\omega}{\varepsilon}(t-\boldsymbol{\kappa}\cdot(\boldsymbol{x}-\boldsymbol{x}_s)+z/c_1(\kappa))}\omega^2 d\boldsymbol{\kappa}d\omega. \quad (3.4)$$

Here the Fourier-transformed Green's function has the form

$$\mathcal{G}^\varepsilon_{\omega,\kappa} = T_{\rm i}(\kappa)\exp\Big(\frac{i\omega}{\varepsilon}\big(\frac{1}{c_0(\kappa)}-\frac{1}{c_1(\kappa)}\big)L_{\rm i}\Big)\Big[1-R_{\rm i}(\kappa)\exp\Big(2\frac{i\omega}{\varepsilon c_0(\kappa)}L_{\rm i}\Big)\Big]^{-1}, \quad (3.5)$$

where

$$R_{\rm i}(\kappa) = \frac{\zeta_0(\kappa)-\zeta_1(\kappa)}{\zeta_1(\kappa)+\zeta_0(\kappa)} \quad \text{and} \quad T_{\rm i}(\kappa) = \frac{2\sqrt{\zeta_0(\kappa)\zeta_1(\kappa)}}{\zeta_1(\kappa)+\zeta_0(\kappa)} \quad (3.6)$$

are the mode-dependent reflection and transmission coefficients of the interface at $z = -L_{\rm i}$. The Green's function can be expanded as

$$\mathcal{G}^\varepsilon_{\omega,\kappa} = T_{\rm i}(\kappa)\exp\Big(-\frac{i\omega}{\varepsilon c_1(\kappa)}L_{\rm i}\Big)\sum_{j=0}^{\infty}R_{\rm i}^j(\kappa)\exp\Big((2j+1)\frac{i\omega}{\varepsilon c_0(\kappa)}L_{\rm i}\Big). \quad (3.7)$$

Each term of the sum can be interpreted as the contribution of the waves reflected back and forth j times between the surface $z = 0$ and the interface $z = -L_{\rm i}$, and finally transmitted through the interface $z = -L_{\rm i}$ and propagated till $z = -L$.

We next consider the pressure field at the position $\vec{\boldsymbol{x}}_q = (\boldsymbol{x}_q, -L)$ with $\boldsymbol{x}_q = \boldsymbol{x}_s$ in the limit $\varepsilon \to 0$. We apply the stationary phase method and find that the value of the integral (3.4) for the j-th multiple is given by the contribution around the stationary slowness vector $\boldsymbol{\kappa}_{{\rm sp},j} = \mathbf{0}$ and is concentrated around the time

$$t_{{\rm sp},j} = \frac{L-L_{\rm i}}{c_1} + \frac{(2j+1)L_{\rm i}}{c_0}, \quad (3.8)$$

which is the travel time of the ray going from the source $\vec{\boldsymbol{x}}_s = (\boldsymbol{x}_s, 0)$ to the observation point $\vec{\boldsymbol{x}}_q = (\boldsymbol{x}_s, -L)$ after j reflections between the surface $z = 0$ and the interface $z = -L_{\rm i}$. Finally, we find that the wave is transmitted in the form of train of short pulses that are received at the travel times $\{t_{{\rm sp},j}, j \in \mathbb{N}\}$ and we have for any $j \in \mathbb{N}$:

$$\lim_{\varepsilon\to 0} p^\varepsilon\big(t_{{\rm sp},j}+\varepsilon s, \vec{\boldsymbol{x}}_q;\vec{\boldsymbol{x}}_s\big) = -\frac{\sqrt{\zeta_1}T_{\rm i}(0)R_{\rm i}^j(0)}{2\pi\sqrt{\zeta_0}[c_1(L-L_{\rm i})+(2j+1)c_0L_{\rm i}]}f_z'(s). \quad (3.9)$$

Beyond the power law decay due to the geometric spreading, the exponential decay of the energies carried by the multiples can be observed due to the factor $R_{\rm i}^j(0)$. This exponential decay is typical of a deterministic interface. Note that the wave front ($j = 0$) possesses a fraction $|T_{\rm i}|^2$ of the total power, and that the multiples have the fraction $|R_{\rm i}|^2 = 1 - |T_{\rm i}|^2$. Therefore, in the case of a strong interface, most of the transmitted power is in the multiples.

We now highlight that some of the particular features of the surface wave energy that originate from the pressure release boundary conditions, and which we have

discussed in the context of a random medium, are also present in the case with a deterministic interface. The square modulus of the Green's function $|\mathcal{G}^{\varepsilon}_{\omega,\kappa}|^2$ is given by

$$|\mathcal{G}^{\varepsilon}_{\omega,\kappa}|^2 = \frac{1-R_{\rm i}^2(\kappa)}{|1-R_{\rm i}(\kappa)\exp\left(2i\frac{\omega}{\varepsilon c_0(\kappa)}L_{\rm i}\right)|^2}, \tag{3.10}$$

where we have used the relation $T_{\rm i}^2(\kappa)=1-R_{\rm i}^2(\kappa)$. For a given slowness κ, the square modulus of the Green's function displays an interesting behavior as a function of the frequency ω. It oscillates periodically between the two extremal values

$$\min_{\omega}|\mathcal{G}^{\varepsilon}_{\omega,\kappa}|^2 = \frac{1-|R_{\rm i}(\kappa)|}{1+|R_{\rm i}(\kappa)|}, \qquad \max_{\omega}|\mathcal{G}^{\varepsilon}_{\omega,\kappa}|^2 = \frac{1+|R_{\rm i}(\kappa)|}{1-|R_{\rm i}(\kappa)|},$$

with the small period $\omega_p = \varepsilon\pi c_0(\kappa)/L_{\rm i}$. The interesting point is that its frequency-average is equal to one whatever the value of the reflectivity of the interface $R_{\rm i}(\kappa)$:

$$\left\langle|\mathcal{G}^{\varepsilon}_{\omega,\kappa}|^2\right\rangle_{\omega} = 1. \tag{3.11}$$

Note that this conservation relation is valid only after frequency averaging, and that the variations of the square modulus of the Green's function within the period are large when the interface is strong $|R_{\rm i}(\kappa)|\sim 1$:

$$\left\langle|\mathcal{G}^{\varepsilon}_{\omega,\kappa}|^4\right\rangle_{\omega} = \frac{1+R_{\rm i}^2(\kappa)}{1-R_{\rm i}^2(\kappa)}. \tag{3.12}$$

Eq. (3.11) shows that the total energy emitted by a broadband source such as (2.6) and received at the surface $z=-L$ does not depend on the reflectivity of the interface. With a weak interface $|R_{\rm i}(\kappa)|\ll 1$, most of the energy is carried by the direct waves (the term $j=0$) which have strong amplitudes. With a strong interface $|R_{\rm i}(\kappa)|\sim 1$, the energy is distributed over a long train of short pulses which have small and exponentially decaying amplitudes. Therefore, although the energy distribution amongst the multiples depends strongly on the interface reflectivity, the total received energy does not.

3.2. Secondary Field. We now assume that there is a point reflector at $\vec{\boldsymbol{y}} = (\boldsymbol{y}, -L_y)$ (see Figure 3.2) and compute the secondary field at $\vec{\boldsymbol{x}}_q = (\boldsymbol{x}_q, -L)$:

$$p_1^{\varepsilon}(t,\vec{\boldsymbol{x}}_q;\vec{\boldsymbol{x}}_s) = \frac{1}{(2\pi)^3\varepsilon}\int \frac{\sqrt{\zeta_1(\kappa)}}{2}\left[\hat{a}_1^{\varepsilon}(\omega,\boldsymbol{\kappa},-L)e^{-i\frac{\omega}{\varepsilon}L/c_1(\kappa)} - \hat{b}_1^{\varepsilon}(\omega,\boldsymbol{\kappa},-L)e^{i\frac{\omega}{\varepsilon}L/c_1(\kappa)}\right] \times e^{-i\frac{\omega}{\varepsilon}(t-\boldsymbol{\kappa}\cdot\boldsymbol{x}_q)}\omega^2 d\omega d\boldsymbol{\kappa}\,, \tag{3.13}$$

with

$$\hat{a}_1^{\varepsilon}(\omega,\boldsymbol{\kappa},-L) = \hat{S}_a^{\varepsilon}(\omega,\boldsymbol{\kappa})\,, \tag{3.14}$$

$$\hat{b}_1^{\varepsilon}(\omega,\boldsymbol{\kappa},-L) = e^{-2i\frac{\omega}{\varepsilon}\frac{L_{\rm i}}{c_1(\kappa)}}\Big(-R_{\rm i}(\kappa) + \frac{T_{\rm i}(\kappa)^2 e^{2i\frac{\omega}{\varepsilon}\frac{L_{\rm i}}{c_0(\kappa)}}}{1-R_{\rm i}(\kappa)e^{2i\frac{\omega}{\varepsilon}\frac{L_{\rm i}}{c_0(\kappa)}}}\Big)\hat{S}_a^{\varepsilon}(\omega,\boldsymbol{\kappa})\,, \tag{3.15}$$

$$\hat{S}_a^{\varepsilon}(\omega,\boldsymbol{\kappa}) = \Big[\frac{\sqrt{\zeta_1(\kappa)}}{\rho_1}\boldsymbol{\kappa}\cdot\hat{\boldsymbol{f}}^{\varepsilon}_{1,\boldsymbol{x}}(\omega;\vec{\boldsymbol{x}}_s) + \frac{1}{\sqrt{\zeta_1(\kappa)}}\hat{f}^{\varepsilon}_{1,z}(\omega;\vec{\boldsymbol{x}}_s)\Big]e^{i\frac{\omega}{\varepsilon}(-\boldsymbol{\kappa}\cdot\boldsymbol{y}+L_y/c_1(\kappa))}\,,$$

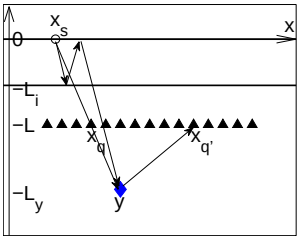

FIG. 3.2. *Emission from a point source located at* $\vec{\boldsymbol{x}}_s = (\boldsymbol{x}_s, 0)$. *The reflector position is* $\vec{\boldsymbol{y}} = (\boldsymbol{y}, -L_y)$. *The receivers are located at depth* $-L$: $\vec{\boldsymbol{x}}_q = (\boldsymbol{x}_q, -L)$ *and* $\vec{\boldsymbol{x}}_{q'} = (\boldsymbol{x}_{q'}, -L)$. *There is an interface at depth* $z = -L_{\rm i}$.

with the secondary source terms given by

$$\hat{\boldsymbol{f}}^{\varepsilon}_{1,\boldsymbol{x}}(\omega;\vec{\boldsymbol{x}}_s) = -\frac{i\sigma_{\rm ref}}{(2\pi)^2\varepsilon}\int \boldsymbol{\kappa}'\frac{\sqrt{\zeta_1(\kappa')}}{\sqrt{\zeta_0(\kappa')}}\mathcal{G}^{\varepsilon}_{\omega,\kappa'}e^{i\frac{\omega}{\varepsilon}(\boldsymbol{\kappa}'\cdot(\boldsymbol{y}-\boldsymbol{x}_s)+L_y/c_1(\kappa'))}\hat{f}_z(\omega)\omega^3 d\boldsymbol{\kappa}', \quad (3.16)$$

$$\hat{f}^{\varepsilon}_{1,z}(\omega;\vec{\boldsymbol{x}}_s) = \frac{i\sigma_{\rm ref}}{(2\pi)^2\varepsilon}\int \frac{\rho_1}{\sqrt{\zeta_0(\kappa')\zeta_1(\kappa')}}\mathcal{G}^{\varepsilon}_{\omega,\kappa'}e^{i\frac{\omega}{\varepsilon}(\boldsymbol{\kappa}'\cdot(\boldsymbol{y}-\boldsymbol{x}_s)+L_y/c_1(\kappa'))}\hat{f}_z(\omega)\omega^3 d\boldsymbol{\kappa}'. \quad (3.17)$$

This gives:

$$p^{\varepsilon}_1(t,\vec{\boldsymbol{x}}_q;\vec{\boldsymbol{x}}_s) = \frac{i\sigma_{\rm ref}}{2(2\pi)^5\varepsilon^2}\int \frac{\sqrt{\zeta_1(\kappa')}}{\sqrt{\zeta_0(\kappa')}}\left(-\frac{\zeta_1(\kappa)\boldsymbol{\kappa}\cdot\boldsymbol{\kappa}'}{\rho_1}+\frac{\rho_1}{\zeta_1(\kappa')}\right)\hat{f}_z(\omega)\omega^5\mathcal{G}^{\varepsilon}_{\omega,\kappa'}$$

$$\times\Big[e^{i\frac{\omega}{\varepsilon}\phi_I(\boldsymbol{\kappa},\boldsymbol{\kappa}')} - \Big(-R_{\rm i}(\kappa)+\frac{T_{\rm i}(\kappa)^2e^{2i\frac{\omega}{\varepsilon}\frac{L_{\rm i}}{c_0(\kappa)}}}{1-R_{\rm i}(\kappa)e^{2i\frac{\omega}{\varepsilon}\frac{L_{\rm i}}{c_0(\kappa)}}}\Big)e^{i\frac{\omega}{\varepsilon}\phi_{II}(\boldsymbol{\kappa},\boldsymbol{\kappa}')}\Big]d\omega d\boldsymbol{\kappa} d\boldsymbol{\kappa}', \quad (3.18)$$

where the two rapid phases are given by:

$$\phi_I(\boldsymbol{\kappa},\boldsymbol{\kappa}') = -t+\boldsymbol{\kappa}\cdot(\boldsymbol{x}_q-\boldsymbol{y})+\frac{L_y-L}{c_1(\kappa)}+\boldsymbol{\kappa}'\cdot(\boldsymbol{y}-\boldsymbol{x}_s)+\frac{L_y}{c_1(\kappa')}, \quad (3.19)$$

$$\phi_{II}(\boldsymbol{\kappa},\boldsymbol{\kappa}') = -t+\boldsymbol{\kappa}\cdot(\boldsymbol{x}_q-\boldsymbol{y})+\frac{L_y+L-2L_{\rm i}}{c_1(\kappa)}+\boldsymbol{\kappa}'\cdot(\boldsymbol{y}-\boldsymbol{x}_s)+\frac{L_y}{c_1(\kappa')}. \quad (3.20)$$

Let us briefly analyze the case in which $\boldsymbol{x}_s = \boldsymbol{x}_q = \boldsymbol{y}$ (the source point, the receiver and the reflector are on the same vertical line) and $L = L_{\rm i}$ (the receiver is at the interface depth). Then the secondary field consists in a sequence of short pulses that arrive at times

$$t_{{\rm sp},j} = 2\frac{L_y-L_{\rm i}}{c_1}+(1+2j)\frac{L_{\rm i}}{c_0},$$

for $j = 0, 1, \ldots$. For $j = 0$ we have

$$p^{\varepsilon}_1(t_{{\rm sp},0}+\varepsilon s,\vec{\boldsymbol{x}}_q;\vec{\boldsymbol{x}}_s) \stackrel{\varepsilon\to 0}{\longrightarrow} -\frac{\sigma_{\rm ref}\sqrt{\zeta_1}}{2(2\pi)^2\sqrt{\zeta_0}c_1}\frac{T_{\rm i}(0)(1+R_{\rm i}(0))}{\big[c_0L_{\rm i}+c_1(L_y-L_{\rm i})\big]\big[c_1(L_y-L_{\rm i})\big]}f^{(3)}_z(s),$$

and for $j = 1$,

$$p^{\varepsilon}_1(t_{{\rm sp},1}+\varepsilon s,\vec{\boldsymbol{x}}_q;\vec{\boldsymbol{x}}_s) \stackrel{\varepsilon\to 0}{\longrightarrow} -\frac{\sigma_{\rm ref}\sqrt{\zeta_1}}{2(2\pi)^2\sqrt{\zeta_0}c_1}\Big[\frac{T_{\rm i}(0)R_{\rm i}(0)(1+R_{\rm i}(0))}{\big[3c_0L_{\rm i}+c_1(L_y-L_{\rm i})\big]\big[c_1(L_y-L_{\rm i})\big]}$$
$$-\frac{T_{\rm i}(0)^2}{\big[c_0L_{\rm i}+c_1(L_y-L_{\rm i})\big]\big[2c_0L_{\rm i}+c_1(L_y-L_{\rm i})\big]}\Big]f^{(3)}_z(s).$$

3.3. The Cross Correlation. From now on we will assume that the receivers are at the interface, which means $L = L_{\rm i}$. This models the situation in geophysics in which sources are at the surface of the sea, and a sensor array records the signals at the surface of the sea bottom. These two interfaces generate a lot of multiples that are problematic for the standard imaging technique.

The secondary cross correlation between $\vec{\boldsymbol{x}}_q$ and $\vec{\boldsymbol{x}}_{q'}$ has a peak centered at the sum of travel times $[|\vec{\boldsymbol{y}} - \vec{\boldsymbol{x}}_q| + |\vec{\boldsymbol{x}}_{q'} - \vec{\boldsymbol{y}}|]/c_1$:

$$\begin{aligned}
&\mathcal{C}^\varepsilon\Big(\frac{|\vec{\boldsymbol{y}} - \vec{\boldsymbol{x}}_q| + |\vec{\boldsymbol{x}}_{q'} - \vec{\boldsymbol{y}}|}{c_1} + \varepsilon s, \vec{\boldsymbol{x}}_q, \vec{\boldsymbol{x}}_{q'}\Big)\\
&\xrightarrow{\varepsilon\to 0} \frac{i\sigma_{\rm ref}}{2(2\pi)^3 c_1^3} \frac{(\vec{\boldsymbol{y}} - \vec{\boldsymbol{x}}_q)\cdot(\vec{\boldsymbol{x}}_{q'} - \vec{\boldsymbol{y}})}{|\vec{\boldsymbol{y}} - \vec{\boldsymbol{x}}_q|^3\,|\vec{\boldsymbol{x}}_{q'} - \vec{\boldsymbol{y}}|^2} \frac{\rho_1\sqrt{c_1^2|\vec{\boldsymbol{y}} - \vec{\boldsymbol{x}}_q|^2 - c_0^2|\boldsymbol{y} - \boldsymbol{x}_q|^2}}{\rho_0 c_0}\\
&\qquad \times \int |\hat{f}_z(\omega)|^2 \omega^3 \exp\big(i\omega s\big) d\omega,
\end{aligned} \tag{3.21}$$

and another peak centered at $-[|\vec{\boldsymbol{y}} - \vec{\boldsymbol{x}}_q| + |\vec{\boldsymbol{x}}_{q'} - \vec{\boldsymbol{y}}|]/c_1$:

$$\begin{aligned}
&\mathcal{C}^\varepsilon\Big(-\frac{|\vec{\boldsymbol{y}} - \vec{\boldsymbol{x}}_q| + |\vec{\boldsymbol{x}}_{q'} - \vec{\boldsymbol{y}}|}{c_1} + \varepsilon s, \vec{\boldsymbol{x}}_q, \vec{\boldsymbol{x}}_{q'}\Big)\\
&\xrightarrow{\varepsilon\to 0} \frac{i\sigma_{\rm ref}}{2(2\pi)^3 c_1^3} \frac{(\vec{\boldsymbol{y}} - \vec{\boldsymbol{x}}_q)\cdot(\vec{\boldsymbol{x}}_{q'} - \vec{\boldsymbol{y}})}{|\vec{\boldsymbol{y}} - \vec{\boldsymbol{x}}_q|^2\,|\vec{\boldsymbol{x}}_{q'} - \vec{\boldsymbol{y}}|^3} \frac{\rho_1\sqrt{c_1^2|\vec{\boldsymbol{x}}_{q'} - \vec{\boldsymbol{y}}|^2 - c_0^2|\boldsymbol{x}_{q'} - \boldsymbol{y}|^2}}{\rho_0 c_0}\\
&\qquad \times \int |\hat{f}_z(\omega)|^2 \omega^3 \exp\big(-i\omega s\big) d\omega.
\end{aligned} \tag{3.22}$$

Note that the amplitudes of these peaks are independent of the transmission/reflection coefficients through the interface. This comes again from the fact that the evaluation of the cross correlation summed over the surface array that covers the plane $z = 0$ involves the integral in frequency of the square modulus $|\mathcal{G}^\varepsilon_{\omega,\kappa}|^2$, which is a periodic function in ω with a small period of order ε and with an average equal to one. That is why the reflectivity of the interface does not appear in the final expression.

3.4. Kirchhoff Migration of Cross Correlations. The analysis of the Kirchhoff migration of the cross correlation matrix then follows the same lines as in the case of a randomly layered medium. The Kirchhoff migration function for the search point $\vec{\boldsymbol{y}}^S$ is defined as in (2.10) by

$$\mathcal{I}^\varepsilon_{\rm C}(\vec{\boldsymbol{y}}^S) = \frac{1}{N_{\rm q}^2} \sum_{q,q'=1}^{N_{\rm q}} \mathcal{C}^\varepsilon\Big(\frac{|\vec{\boldsymbol{x}}_q - \vec{\boldsymbol{y}}^S| + |\vec{\boldsymbol{y}}^S - \vec{\boldsymbol{x}}_{q'}|}{c_1}, \vec{\boldsymbol{x}}_q, \vec{\boldsymbol{x}}_{q'}\Big), \tag{3.23}$$

where $N_{\rm q}$ is the number of receivers at the auxiliary array. If the receiver array at depth $-L$ is a dense square array centered at $\boldsymbol{x}_A$ and with sidelength a, then, denoting the search point by $\vec{\boldsymbol{y}}^S = \vec{\boldsymbol{y}} + (\boldsymbol{\xi}, \eta)$, we have

$$\begin{aligned}
\mathcal{I}^\varepsilon_{\rm C}(\vec{\boldsymbol{y}}^S) &\xrightarrow{\varepsilon\to 0} \frac{i\sigma_{\rm ref}}{2(2\pi)^3 c_1^3 (L_y - L)^2} \mathrm{sinc}^2\Big(\frac{\pi a\xi_1}{\lambda_1(L_y - L)}\Big)\mathrm{sinc}^2\Big(\frac{\pi a\xi_2}{\lambda_1(L_y - L)}\Big)\\
&\qquad \times \int \omega^3 |\hat{f}_z(\omega)|^2 \exp\Big(2i\frac{\omega}{c_1}(\eta + \boldsymbol{\xi}\cdot\frac{\boldsymbol{x}_A - \boldsymbol{y}}{L_y - L})\Big) d\omega.
\end{aligned} \tag{3.24}$$

Here we have simplified the expression by assuming Hypothesis (2.12) and the central wavelength is $\lambda_1 = 2\pi c_1/\omega_0$.

4. Imaging through a Random Medium in the Paraxial Regime. In this section we analyze a scaling regime in which scattering is isotropic and weak, which allows us to use the random paraxial wave model to describe the wave propagation in the scattering region. In this approximation, backscattering is negligible but there is significant lateral scattering as the wave advances and over long propagation distances. Even though they are weak, these effects accumulate and can be a limiting factor in imaging and communications if not mitigated in some way. Wave propagation in random media in the paraxial regime has been used extensively in underwater sound propagation as well as in the microwave and optical regimes in the atmosphere [28, 39, 38, 26]. We formulate the regime of paraxial wave propagation in random media with a scaling of parameters that allows detailed and effective mathematical analysis [23]. It is described as follows.

1) We assume that the correlation length l_c of the medium is much smaller than the typical propagation distance L. We denote by ε^2 the ratio between the correlation length and the typical propagation distance:

$$\frac{l_c}{L} \sim \varepsilon^2.$$

2) We assume that the transverse width of the source R_0 and the correlation length of the medium l_c are of the same order. This means that the ratio R_0/L is of order ε^2. This scaling is motivated by the fact that, in this regime, there is a non-trivial interaction between the fluctuations of the medium and the beam.

3) We assume that the typical wavelength λ is much smaller than the propagation distance L, more precisely, we assume that the ratio λ/L is of order ε^4. This high-frequency scaling is motivated by the following considerations. The Rayleigh length for a beam with initial width R_0 and central wavelength λ is of the order of R_0^2/λ when there is no random fluctuation (the Rayleigh length is the distance from beam waist where the beam area is doubled by diffraction). In order to get a Rayleigh length of the order of the propagation distance L, the ratio λ/L must be of order ε^4 since $R_0/L \sim \varepsilon^2$:

$$\frac{\lambda}{L} \sim \varepsilon^4.$$

4) We assume that the typical amplitude of the random fluctuations of the medium is small. More exactly, we assume that the relative amplitude of the fluctuations is of order ε^3. This scaling has been chosen so as to obtain an effective regime of order one when ε goes to zero. That is, if the magnitude of the fluctuations is smaller than ε^3, then the wave would propagate as if the medium was homogeneous, while if the order of magnitude is larger, then the wave would not be able to penetrate the random medium. The scaling that we consider here corresponds to the physically most interesting situation.

4.1. The Random Paraxial Wave Equation. We consider the time-harmonic form of the scalar wave equation

$$(\partial_z^2 + \Delta_\perp)\hat{p} + \frac{\omega^2}{c_0^2}\big(1 + \mu(\boldsymbol{x}, z)\big)\hat{p} = 0. \tag{4.1}$$

Here μ is a zero-mean, stationary, three-dimensional random process with mixing properties in the z-direction. In the high-frequency regime described above,

$$\omega \to \frac{\omega}{\varepsilon^4}, \qquad \mu(\boldsymbol{x}, z) \to \varepsilon^3 \mu\big(\frac{\boldsymbol{x}}{\varepsilon^2}, \frac{z}{\varepsilon^2}\big), \tag{4.2}$$

the rescaled function ϕ^ε defined by

$$\hat{p}^\varepsilon(\omega,\boldsymbol{x},z)=\exp\Big(i\frac{\omega}{\varepsilon^4}\frac{z}{c_0}\Big)\phi^\varepsilon\Big(\frac{\omega}{\varepsilon^4},\frac{\boldsymbol{x}}{\varepsilon^2},z\Big)$$

satisfies

$$\partial_z^2\phi^\varepsilon+\frac{1}{\varepsilon^4}\left(2i\frac{\omega}{c_0}\partial_z\phi^\varepsilon+\Delta_\perp\phi^\varepsilon+\frac{\omega^2}{\varepsilon c_0^2}\mu\big(\boldsymbol{x},\frac{z}{\varepsilon^2}\big)\phi^\varepsilon\right)=0.$$

In the regime $\varepsilon\ll 1$, it has been shown in [23] that the forward-scattering approximation in direction z is valid and the function ϕ^ε can be considered to satisfy the Schrödinger-type equation

$$2i\frac{\omega}{c_0}\partial_z\phi^\varepsilon+\Delta_\perp\phi^\varepsilon+\frac{\omega^2}{\varepsilon c_0^2}\mu\big(\boldsymbol{x},\frac{z}{\varepsilon^2}\big)\phi^\varepsilon=0.$$

Note that the random potential in this Schrödinger equation has the form of a white noise in z, i.e. $\frac{1}{\varepsilon}\mu(\frac{z}{\varepsilon^2})$, which explains the choice of the amplitude ε^3 for the perturbation of the index of refraction in (4.2). We introduce the fundamental solution $\hat{G}^\varepsilon\big(\omega,(\boldsymbol{x},z),(\boldsymbol{x}_0,z_0)\big)$:

$$2i\frac{\omega}{c_0}\partial_z\hat{G}^\varepsilon+\Delta_\perp\hat{G}^\varepsilon+\frac{\omega^2}{\varepsilon c_0^2}\mu(\boldsymbol{x},\frac{z}{\varepsilon^2})\hat{G}^\varepsilon=0, \tag{4.3}$$

starting from $\hat{G}^\varepsilon\big(\omega,(\boldsymbol{x},z=z_0),(\boldsymbol{x}_0,z_0)\big)=\delta(\boldsymbol{x}-\boldsymbol{x}_0)$. In a homogeneous medium ($\mu\equiv 0$) the fundamental solution is

$$\hat{G}_0\big(\omega,(\boldsymbol{x},z),(\boldsymbol{x}_0,z_0)\big)=\frac{\omega}{2i\pi c_0|z-z_0|}\exp\Big(i\frac{\omega|\boldsymbol{x}-\boldsymbol{x}_0|^2}{2c_0|z-z_0|}\Big). \tag{4.4}$$

In a random medium and in the scaling regime described above, the first two moments of the random fundamental solution have the following behaviors.

PROPOSITION 4.1. *The first order-moment of the random fundamental solution exhibits frequency-dependent damping:*

$$\mathbb{E}\big[\hat{G}^\varepsilon\big(\omega,(\boldsymbol{x},z),(\boldsymbol{x}_0,z_0)\big)\big]\overset{\varepsilon\to 0}{\longrightarrow}\hat{G}_0\big(\omega,(\boldsymbol{x},z),(\boldsymbol{x}_0,z_0)\big)\exp\Big(-\frac{\gamma_0(\mathbf{0})\omega^2|z-z_0|}{8c_0^2}\Big), \tag{4.5}$$

where $\gamma_0(\boldsymbol{x})=\int_{-\infty}^{\infty}\mathbb{E}[\mu(\mathbf{0},0)\mu(\boldsymbol{x},z)]dz$.

The second order-moment of the random fundamental solution exhibits spatial decorrelation:

$$\begin{aligned}&\mathbb{E}\big[\hat{G}^\varepsilon\big(\omega,(\boldsymbol{x},z),(\boldsymbol{x}_0,z_0)\big)\overline{\hat{G}^\varepsilon\big(\omega,(\boldsymbol{x}',z),(\boldsymbol{x}_0,z_0)\big)}\big]\\&\overset{\varepsilon\to 0}{\longrightarrow}\hat{G}_0\big(\omega,(\boldsymbol{x},z),(\boldsymbol{x}_0,z_0)\big)\overline{\hat{G}_0\big(\omega,(\boldsymbol{x}',z),(\boldsymbol{x}_0,z_0)\big)}\exp\Big(-\frac{\omega^2|z-z_0|\gamma_2(\boldsymbol{x}-\boldsymbol{x}')}{4c_0^2}\Big),\end{aligned} \tag{4.6}$$

where $\gamma_2(\boldsymbol{x})=\int_0^1\gamma_0(\mathbf{0})-\gamma_0(\boldsymbol{x}s)ds$.

These are classical results [27, Chapter 20] once the the random paraxial equation has been proved to be correct, as is the case here. The result on the first-order moment shows that any coherent wave imaging method cannot give good images if the propagation distance is larger than the scattering mean free path $l_{\rm sca}=8c_0^2/(\gamma_0(\mathbf{0})\omega^2)$, because the coherent wave components will then be exponentially damped. This is the situation we have in mind, and this is the situation in which imaging by migration of cross correlations turns out to be efficient. The results on the second-order moment will be used in the next subsection to analyse the cross correlation of the recorded signals in a quantitative way.

4.2. The Cross Correlation of Recorded Field in the Presence of a Reflector. We consider the situation in which the medium is random in the region $z \in (-L, 0)$ and there is a reflector below the random medium placed at $\vec{\boldsymbol{y}} = (\boldsymbol{y}, -L_y)$, $L_y > L$ (see Figure 1.2). Assume that there are point sources at the surface array $(\vec{\boldsymbol{x}}_s)_{s=1}^{N_s}$, where $\vec{\boldsymbol{x}}_s = (\boldsymbol{x}_s, 0)$. When the source at $\vec{\boldsymbol{x}}_s$ emits the scaled pulse $f(t/\varepsilon^4)$, the signals $p^\varepsilon(t, \vec{\boldsymbol{x}}_q; \vec{\boldsymbol{x}}_s)$ are recorded at the points $(\vec{\boldsymbol{x}}_q)_{q=1}^{N_q}$ of an auxiliary array, where $\vec{\boldsymbol{x}}_q = (\boldsymbol{x}_q, -L)$. We consider the cross correlation of the signals recorded at the auxiliary array defined by:

$$\mathcal{C}^\varepsilon\big(\tau, \vec{\boldsymbol{x}}_q, \vec{\boldsymbol{x}}_{q'}\big) = \int_0^T \sum_{s=1}^{N_s} p^\varepsilon(t, \vec{\boldsymbol{x}}_q; \vec{\boldsymbol{x}}_s) p^\varepsilon(t+\tau, \vec{\boldsymbol{x}}_{q'}; \vec{\boldsymbol{x}}_s) dt. \tag{4.7}$$

Using the Born approximation for the point reflector at $\vec{\boldsymbol{y}}$, we obtain the following proposition.

PROPOSITION 4.2. *In the random paraxial wave regime $\varepsilon \to 0$, when there is a point reflector at $\vec{\boldsymbol{y}} = (\boldsymbol{y}, -L_y)$, then the cross correlation of the recorded signals at the auxiliary array satisfies*

$$\begin{aligned}\mathcal{C}^\varepsilon\Big(\frac{2L_y - 2L}{c_0} + \varepsilon^4 s, \vec{\boldsymbol{x}}_q, \vec{\boldsymbol{x}}_{q'}\Big) \overset{\varepsilon\to 0}{\longrightarrow} -\frac{i\sigma_{\rm ref}}{4\pi^3 c_0 (L_y - L)^2} \int \omega^3 |\hat f(\omega)|^2 \\ \times \exp\Big(- i\omega\big(s - \frac{1}{2c_0} \frac{|\boldsymbol{y} - \boldsymbol{x}_q|^2 + |\boldsymbol{y} - \boldsymbol{x}_{q'}|^2}{L_y - L}\big)\Big) d\omega. \end{aligned} \tag{4.8}$$

This shows that
- the cross correlation has a peak at time lag $\tau = \frac{2L_y - 2L}{c_0} + \frac{\varepsilon^4}{2c_0} \frac{|\boldsymbol{y} - \boldsymbol{x}_q|^2 + |\boldsymbol{y} - \boldsymbol{x}_{q'}|^2}{L_y - L}$, which is the sum of travel times from $\vec{\boldsymbol{x}}_q$ to $\vec{\boldsymbol{y}}$ and from $\vec{\boldsymbol{y}}$ to $\vec{\boldsymbol{x}}_{q'}$ in the paraxial approximation:

$$\begin{aligned}\mathcal{T}(\vec{\boldsymbol{x}}_q, \vec{\boldsymbol{y}}) + \mathcal{T}(\vec{\boldsymbol{y}}, \vec{\boldsymbol{x}}_{q'}) &= \frac{1}{c_0}\sqrt{(L_y - L)^2 + \varepsilon^4 |\boldsymbol{y} - \boldsymbol{x}_q|^2} + \frac{1}{c_0}\sqrt{(L_y - L)^2 + \varepsilon^4 |\boldsymbol{y} - \boldsymbol{x}_{q'}|^2} \\ &= \frac{2L_y - 2L}{c_0} + \frac{\varepsilon^4}{2c_0} \frac{|\boldsymbol{y} - \boldsymbol{x}_q|^2 + |\boldsymbol{y} - \boldsymbol{x}_{q'}|^2}{L_t - L} + O(\varepsilon^8).\end{aligned}$$

- the effect of the random medium has completely disappeared.

The conclusion is therefore that Kirchhoff migration with cross correlations of the auxiliary array produces images as if the medium was homogeneous and the auxiliary array was active. We formulate this result in the next subsection.

Proof. We first describe the different wave signals that can be recorded at the surface array or at the auxiliary array.

1) The field recorded at the auxiliary passive array at $\vec{\boldsymbol{x}}_q = (\boldsymbol{x}_q, -L)$ around time L/c_0 is the field transmitted through the scattering layer in $z \in (-L, 0)$:

$$p^\varepsilon\big(\frac{L}{c_0} + \varepsilon^4 s, \vec{\boldsymbol{x}}_q; \vec{\boldsymbol{x}}_s\big) = \frac{1}{2\pi} \int \hat f(\omega) e^{-i\omega s} \hat G^\varepsilon\big(\omega, (\boldsymbol{x}_q, -L), (\boldsymbol{x}_s, 0)\big) d\omega.$$

2) Using the Born approximation for the reflector, the field recorded at the surface array at $\vec{\boldsymbol{x}}_r = (\boldsymbol{x}_r, 0)$ around time $2L_y/c_0$ is of the form

$$\begin{aligned}&p^\varepsilon\big(\frac{2L_y}{c_0} + \varepsilon^4 s, \vec{\boldsymbol{x}}_r; \vec{\boldsymbol{x}}_s\big) = \frac{i\sigma_{\rm ref} c_0}{\pi} \iiint \omega \hat f(\omega) e^{-i\omega s} \hat G^\varepsilon\big(\omega, (\boldsymbol{x}_r, 0), (\boldsymbol{x}', -L)\big) \\ &\times \hat G_0\big(\omega, (\boldsymbol{x}', -L), (\boldsymbol{y}, -L_y)\big) \hat G_0\big(\omega, (\boldsymbol{y}, -L_y), (\boldsymbol{x}, -L)\big) \hat G^\varepsilon\big(\omega, (\boldsymbol{x}, -L), (\boldsymbol{x}_s, 0)\big) d\boldsymbol{x} d\boldsymbol{x}' d\omega.\end{aligned}$$

Using the reciprocity this also reads

$$p^\varepsilon\big(\frac{2L_y}{c_0}+\varepsilon^4 s,\vec{\boldsymbol{x}}_r;\vec{\boldsymbol{x}}_s\big)=\frac{i\sigma_{\rm ref}c_0}{\pi}\iiint\omega\hat f(\omega)e^{-i\omega s}\hat G^\varepsilon\big(\omega,(\boldsymbol{x}',-L),(\boldsymbol{x}_r,0)\big)$$
$$\times\hat G_0\big(\omega,(\boldsymbol{y},-L_y),(\boldsymbol{x}',-L)\big)\hat G_0\big(\omega,(\boldsymbol{y},-L_y),(\boldsymbol{x},-L)\big)\hat G^\varepsilon\big(\omega,(\boldsymbol{x},-L),(\boldsymbol{x}_s,0)\big)d\boldsymbol{x}d\boldsymbol{x}'d\omega.$$

There is no other wave component recorded at $\vec{\boldsymbol{x}}_r$ around a time $t_0\neq 2L_y/c_0$.
3) The field recorded at the auxiliary passive array at $\vec{\boldsymbol{x}}_{q'}=(\boldsymbol{x}_{q'},-L)$ around time $(2L_y-L)/c_0$ is of the form

$$p^\varepsilon\big(\frac{2L_y-L}{c_0}+\varepsilon^4 s,\vec{\boldsymbol{x}}_{q'};\vec{\boldsymbol{x}}_s\big)=\frac{i\sigma_{\rm ref}c_0}{\pi}\iint\omega\hat f(\omega)e^{-i\omega s}\hat G_0\big(\omega,(\boldsymbol{y},-L_y),(\boldsymbol{x}_{q'},-L)\big)$$
$$\times\hat G_0\big(\omega,(\boldsymbol{y},-L_y),(\boldsymbol{x},-L)\big)\hat G^\varepsilon\big(\omega,(\boldsymbol{x},-L),(\boldsymbol{x}_s,0)\big)d\boldsymbol{x}d\omega.$$

In the Born approximation there is no other wave component recorded at $\vec{\boldsymbol{x}}_{q'}$ around a time $t_0\notin\{L/c_0,(2L_y-L)/c_0\}$.
As a consequence the cross correlation of the signals recorded at the auxiliary array defined by (4.7) is concentrated around time lag $2(L_y-L)/c_0$ and it is of the form

$$\mathcal{C}^\varepsilon\big(\frac{2L_y-2L}{c_0}+\varepsilon^4 s,\vec{\boldsymbol{x}}_q,\vec{\boldsymbol{x}}_{q'}\big)=\frac{i\sigma_{\rm ref}c_0}{\pi}\iiint\omega|\hat f(\omega)|^2e^{-i\omega s}\hat G_0\big(\omega,(\boldsymbol{y},-L_y),(\boldsymbol{x}_{q'},-L)\big)$$
$$\times\hat G_0\big(\omega,(\boldsymbol{y},-L_y),(\boldsymbol{x},-L)\big)\hat G^\varepsilon\big(\omega,(\boldsymbol{x},-L),(\boldsymbol{x}_s,0)\big)\overline{\hat G^\varepsilon\big(\omega,(\boldsymbol{x}_q,-L),(\boldsymbol{x}_s,0)\big)}d\boldsymbol{x}_s d\boldsymbol{x}d\omega,$$

when the source array is dense and covers the full surface $z=0$. Using Proposition 4.1 and the self-averaging property of the product of two fundamental solutions (one of them being complex conjugated) [33, 34, 23] we get

$$\mathcal{C}^\varepsilon\big(\frac{2L_y-2L}{c_0}+\varepsilon^4 s,\vec{\boldsymbol{x}}_q,\vec{\boldsymbol{x}}_{q'}\big)\overset{\varepsilon\to0}{\longrightarrow}\frac{i\sigma_{\rm ref}c_0}{\pi}\iiint\omega|\hat f(\omega)|^2e^{-i\omega s}\hat G_0\big(\omega,(\boldsymbol{y},-L_y),(\boldsymbol{x}_{q'},-L)\big)$$
$$\times\hat G_0\big(\omega,(\boldsymbol{y},-L_y),(\boldsymbol{x},-L)\big)\hat G_0\big(\omega,(\boldsymbol{x},-L),(\boldsymbol{x}_s,0)\big)\overline{\hat G_0\big(\omega,(\boldsymbol{x}_q,-L),(\boldsymbol{x}_s,0)\big)}$$
$$\times\exp\Big(-\frac{\omega^2L\gamma_2(\boldsymbol{x}-\boldsymbol{x}_q)}{4c_0^2}\Big)d\boldsymbol{x}_s d\boldsymbol{x}d\omega.$$

Using the explicit expression (4.4) and integrating in $\boldsymbol{x}_s$, it appears a Dirac distribution $\delta(\boldsymbol{x}-\boldsymbol{x}_q)$. The exponential damping term then disappears because $\gamma_2(\boldsymbol{0})=0$ and we finally obtain (4.8). □

4.3. Kirchhoff Migration of Cross Correlations. The Kirchhoff migration function for the search point $\vec{\boldsymbol{y}}^S$ is

$$\mathcal{I}^\varepsilon_{\rm C}(\vec{\boldsymbol{y}}^S)=\frac{1}{N_{\rm q}^2}\sum_{q,q'=1}^{N_{\rm q}}\mathcal{C}^\varepsilon\Big(\frac{|\vec{\boldsymbol{x}}_q-\vec{\boldsymbol{y}}^S|+|\vec{\boldsymbol{y}}^S-\vec{\boldsymbol{x}}_{q'}|}{c_0},\vec{\boldsymbol{x}}_q,\vec{\boldsymbol{x}}_{q'}\Big),\tag{4.9}$$

where $N_{\rm q}$ is the number of receivers at the auxiliary array.

If the receiver array at depth $-L$ is a dense square array centered at $\boldsymbol{0}$ and with sidelength a, then, denoting the search point by

$$\vec{\boldsymbol{y}}^S=\vec{\boldsymbol{y}}+(\varepsilon^2\boldsymbol{\xi},\varepsilon^4\eta),\tag{4.10}$$

we have

$$\mathcal{I}_{\rm C}^{\varepsilon}(\vec{\boldsymbol{y}}^S) \stackrel{\varepsilon\to 0}{\longrightarrow} -\frac{i\sigma_{\rm ref}}{4\pi^3 c_0(L_y-L)^2}\int \omega^3|\hat{f}(\omega)|^2\exp\Big(2i\frac{\omega}{c_0}\eta\Big) \\ \times{\rm sinc}^2\Big(\frac{a\xi_1\omega}{2c_0(L_y-L)}\Big){\rm sinc}^2\Big(\frac{a\xi_2\omega}{2c_0(L_y-L)}\Big)d\omega. \tag{4.11}$$

Assuming Hypothesis (2.12) we have

$$\mathcal{I}_{\rm C}^{\varepsilon}(\vec{\boldsymbol{y}}^S) \stackrel{\varepsilon\to 0}{\longrightarrow} -\frac{i\sigma_{\rm ref}}{4\pi^3 c_0(L_y-L)^2}{\rm sinc}^2\Big(\frac{\pi a\xi_1}{\lambda_0(L_y-L)}\Big){\rm sinc}^2\Big(\frac{\pi a\xi_2}{\lambda_0(L_y-L)}\Big) \\ \times\int \omega^3|\hat{f}(\omega)|^2\exp\Big(2i\frac{\omega}{c_0}\eta\Big)d\omega. \tag{4.12}$$

This shows that the migration of the cross correlation migration gives the same result as if we were migrating the array response matrix of the auxiliary array (see Appendix B). Indeed the imaging function (4.12) is exactly the imaging function that we would obtain if the medium were homogeneous, if the auxiliary receiver array could be used as an active array, and if the response matrix of the auxiliary array were migrated to the search point $\vec{\boldsymbol{y}}^S$. In particular the cross range resolution is $\lambda_0(L-L_y)/a$ and the range resolution is c_0/B.

5. Conclusion. In this paper we have shown in different strongly scattering situations that the data recorded at a passive receiver array can be used in order to improve migration techniques. As already noted, the kind of surface-auxiliary array imaging configuration that we consider here, with and without scattering media and interfaces, has been applied successfully in exploration geophysics. It is also of interest, however, in other applications in imaging where mitigating the effects of strong scattering is needed and could be implemented with the use of auxiliary passive arrays. One such case is in high-frequency radar imaging where the "surface" source array is near the ground, the auxiliary array is on a moving platform above the troposphere, and the reflectors to be imaged are near-orbit satellites.

Acknowledgements. The authors thank the Institut des Hautes Études Scientifiques (IHÉS) for its hospitality while part of this work was done. The work of G. Papanicolaou was supported in part by AFOSR grant FA9550-11-1-0266. The work of J. Garnier was supported in part by ERC Advanced Grant Project MULTIMOD-267184.

Appendix A. Derivation of the Integral Representations of the Fields in a Randomly Layered Medium. We consider the general model (2.3-2.4) for the parameters of the random medium. We use the same approach as in [18, page 369] applying a propagator formulation. We first take a scaled Fourier transform in time and transverse spatial coordinates:

$$\hat{p}^{\varepsilon}(\omega,\boldsymbol{\kappa},z) = \int p^{\varepsilon}(t,\boldsymbol{x},z)e^{i\frac{\omega}{\varepsilon}(t-\boldsymbol{\kappa}\cdot\boldsymbol{x})}dtd\boldsymbol{x}, \tag{A.1}$$

$$\hat{u}^{\varepsilon}(\omega,\boldsymbol{\kappa},z) = \int u^{\varepsilon}(t,\boldsymbol{x},z)e^{i\frac{\omega}{\varepsilon}(t-\boldsymbol{\kappa}\cdot\boldsymbol{x})}dtd\boldsymbol{x}. \tag{A.2}$$

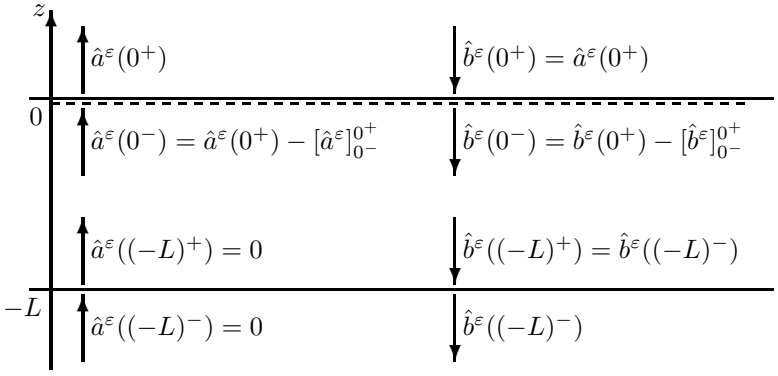

FIG. A.1. *Boundary conditions for the wave modes with a source at $z = 0^-$, a preasure release boundary condition at $z = 0^+$, and a radiation conditions at $-\infty$ (there is no reflector below $z = -L$ here).*

We introduce the up- and down-going modes defined by

$$\hat{a}^\varepsilon(\omega, \boldsymbol{\kappa}, z) = \Big(\frac{1}{\sqrt{\zeta_0(\kappa)}}\hat{p}^\varepsilon(\omega, \boldsymbol{\kappa}, z) + \sqrt{\zeta_0(\kappa)}\hat{u}^\varepsilon(\omega, \boldsymbol{\kappa}, z)\Big)e^{-i\frac{\omega}{\varepsilon}\frac{z}{c_0(\kappa)}}, \tag{A.3}$$

$$\hat{b}^\varepsilon(\omega, \boldsymbol{\kappa}, z) = \Big(-\frac{1}{\sqrt{\zeta_0(\kappa)}}\hat{p}^\varepsilon(\omega, \boldsymbol{\kappa}, z) + \sqrt{\zeta_0(\kappa)}\hat{u}^\varepsilon(\omega, \boldsymbol{\kappa}, z)\Big)e^{i\frac{\omega}{\varepsilon}\frac{z}{c_0(\kappa)}}. \tag{A.4}$$

The pressure release boundary conditions at the surface $z = 0^+$ is $\hat{p}^\varepsilon = 0$, or equivalently (see Figure A.1)

$$\hat{a}^\varepsilon(\omega, \boldsymbol{\kappa}, 0^+) = \hat{b}^\varepsilon(\omega, \boldsymbol{\kappa}, 0^+). \tag{A.5}$$

A.1. Derivation of (2.17-2.18). We consider the situation with a point source at $\vec{\boldsymbol{x}}_s = (\boldsymbol{x}_s, 0)$. The jump conditions across the source plane at $z = 0$ are

$$\big[\hat{p}^\varepsilon\big]_{0^-}^{0^+} = \varepsilon^2\hat{f}_z(\omega)e^{-i\frac{\omega}{\varepsilon}\boldsymbol{\kappa}\cdot\boldsymbol{x}_s}, \qquad \big[\hat{u}^\varepsilon\big]_{0^-}^{0^+} = \frac{\varepsilon^2}{\rho_0}\boldsymbol{\kappa}\cdot\hat{\boldsymbol{f}}_{\boldsymbol{x}}(\omega)e^{-i\frac{\omega}{\varepsilon}\boldsymbol{\kappa}\cdot\boldsymbol{x}_s},$$

which give:

$$\big[\hat{a}^\varepsilon\big]_{0^-}^{0^+} = \varepsilon^2\Big(\frac{\hat{f}_z(\omega)}{\sqrt{\zeta_0(\kappa)}} + \frac{\sqrt{\zeta_0(\kappa)}}{\rho_0}\boldsymbol{\kappa}\cdot\hat{\boldsymbol{f}}_{\boldsymbol{x}}(\omega)\Big)e^{-i\frac{\omega}{\varepsilon}\boldsymbol{\kappa}\cdot\boldsymbol{x}_s}, \tag{A.6}$$

$$\big[\hat{b}^\varepsilon\big]_{0^-}^{0^+} = \varepsilon^2\Big(-\frac{\hat{f}_z(\omega)}{\sqrt{\zeta_0(\kappa)}} + \frac{\sqrt{\zeta_0(\kappa)}}{\rho_0}\boldsymbol{\kappa}\cdot\hat{\boldsymbol{f}}_{\boldsymbol{x}}(\omega)\Big)e^{-i\frac{\omega}{\varepsilon}\boldsymbol{\kappa}\cdot\boldsymbol{x}_s}, \tag{A.7}$$

Using (A.5):

$$\hat{a}^\varepsilon(\omega, \boldsymbol{\kappa}, 0^-) - \hat{b}^\varepsilon(\omega, \boldsymbol{\kappa}, 0^-) = -2\varepsilon^2\frac{\hat{f}_z(\omega)}{\sqrt{\zeta_0(\kappa)}}e^{-i\frac{\omega}{\varepsilon}\boldsymbol{\kappa}\cdot\boldsymbol{x}_s}. \tag{A.8}$$

We also have the radiation condition at $z = -L$:

$$\hat{a}^\varepsilon(\omega, \boldsymbol{\kappa}, -L) = 0. \tag{A.9}$$

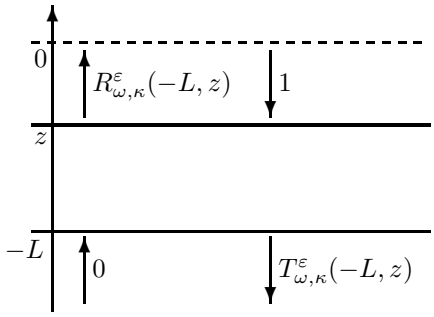

FIG. A.2. *Reflection and transmission coefficients.*

We introduce the propagator matrix, that is the matrix such that, for any $-L < z_0 \leq z \leq 0$:

$$\mathbf{P}^\varepsilon(\omega,\boldsymbol{\kappa},z_0,z)\begin{bmatrix}\hat{a}^\varepsilon(\omega,\boldsymbol{\kappa},z_0)\\ \hat{b}^\varepsilon(\omega,\boldsymbol{\kappa},z_0)\end{bmatrix} = \begin{bmatrix}\hat{a}^\varepsilon(\omega,\boldsymbol{\kappa},z)\\ \hat{b}^\varepsilon(\omega,\boldsymbol{\kappa},z)\end{bmatrix}. \tag{A.10}$$

It is the solution of the linear system

$$\frac{d\mathbf{P}^\varepsilon}{dz} = \mathbf{M}^\varepsilon(\omega,\kappa,z)\mathbf{P}^\varepsilon, \tag{A.11}$$

with the initial condition $\mathbf{P}^\varepsilon(\omega,\boldsymbol{\kappa},z_0,z=z_0)=\mathbf{I}$. Here the entries of the 2×2 matrix $\mathbf{M}^\varepsilon(\omega,\kappa,z)$ are given by

$$M^\varepsilon_{11} = \frac{i\omega c_0(\kappa)}{2c_0^2\varepsilon}\nu\big(\frac{z}{\varepsilon^2}\big), \qquad M^\varepsilon_{21} = M^\varepsilon_{11}e^{2i\frac{\omega}{\varepsilon}\frac{z}{c_0(\kappa)}}, \qquad M^\varepsilon_{12} = \overline{M^\varepsilon_{21}}, \qquad M^\varepsilon_{22} = \overline{M^\varepsilon_{11}}.$$

Note that $\mathbf{P}^\varepsilon(\omega,\boldsymbol{\kappa},z_0,z)$ depends on $\boldsymbol{\kappa}$ only through the modulus $\kappa=|\boldsymbol{\kappa}|$.

We introduce the transmission and reflection coefficients $(T^\varepsilon_{\omega,\kappa}, R^\varepsilon_{\omega,\kappa})$ defined by the relation

$$\mathbf{P}^\varepsilon(\omega,\kappa,-L,z)\begin{bmatrix}0\\ T^\varepsilon_{\omega,\kappa}(-L,z)\end{bmatrix} = \begin{bmatrix}R^\varepsilon_{\omega,\kappa}(-L,z)\\ 1\end{bmatrix}, \tag{A.12}$$

which corresponds to the scattering problem for a unit-power incident plane wave incoming from the half-space (z,∞) and probing the inhomogeneous layer in $(-L,z)$ with transparent boundary conditions (see Figure A.2). By inverting this matrix-vector relation we get

$$T^\varepsilon_{\omega,\kappa}(-L,z) = \frac{1}{P^\varepsilon_{22}(\omega,\kappa,-L,z)}, \qquad R^\varepsilon_{\omega,\kappa}(-L,z) = \frac{P^\varepsilon_{12}(\omega,\kappa,-L,z)}{P^\varepsilon_{22}(\omega,\kappa,-L,z)}. \tag{A.13}$$

From the relation (A.10) evaluated at $z=0^-$ and $z_0=-L$, we get using (A.8) and (A.9)

$$\begin{aligned}\hat{b}^\varepsilon(\omega,\boldsymbol{\kappa},-L) &= \frac{1}{P^\varepsilon_{22}(\omega,\kappa,-L,0)-P^\varepsilon_{12}(\omega,\kappa,-L,0)}2\varepsilon^2\frac{\hat{f}_z(\omega)}{\sqrt{\zeta_0(\kappa)}}e^{-i\frac{\omega}{\varepsilon}\boldsymbol{\kappa}\cdot\boldsymbol{x}_s}\\ &= \frac{T^\varepsilon_{\omega,\kappa}(-L,0)}{1-R^\varepsilon_{\omega,\kappa}(-L,0)}2\varepsilon^2\frac{\hat{f}_z(\omega)}{\sqrt{\zeta_0(\kappa)}}e^{-i\frac{\omega}{\varepsilon}\boldsymbol{\kappa}\cdot\boldsymbol{x}_s},\end{aligned} \tag{A.14}$$

From (A.3-A.4) and the radiation condition (A.9) we obtain for $z \leq -L$:

$$\hat{p}^\varepsilon(\omega,\boldsymbol{\kappa},z) = -\frac{\sqrt{\zeta_0(\kappa)}}{2}\hat{b}^\varepsilon(\omega,\boldsymbol{\kappa},-L)e^{-i\frac{\omega}{\varepsilon}\frac{z}{c_0(\kappa)}},$$
$$\hat{u}^\varepsilon(\omega,\boldsymbol{\kappa},z) = \frac{1}{2\sqrt{\zeta_0(\kappa)}}\hat{b}^\varepsilon(\omega,\boldsymbol{\kappa},-L)e^{-i\frac{\omega}{\varepsilon}\frac{z}{c_0(\kappa)}}.$$

Substituting (A.14) into these equations give (2.17-2.18) with (2.20).

If the medium is homogeneous $\nu \equiv 0$, then the propagator matrix is equal to the identity matrix and we obtain from (A.14):

$$\hat{b}^\varepsilon(\omega,\boldsymbol{\kappa},-L) = 2\varepsilon^2\frac{\hat{f}_z(\omega)}{\sqrt{\zeta_0(\kappa)}}.$$

This expression gives (2.21) in Section 2.4.2.

A.2. Derivation of (2.26). We consider the same situation as in the previous subsection and we compute the vertical velocity field at the surface. Substituting (A.9) and (A.14) into the relation (A.10) evaluated at $z = 0^-$ and $z_0 = -L$ we obtain:

$$\hat{a}^\varepsilon(\omega,\boldsymbol{\kappa},0^-) = \frac{2R^\varepsilon_{\omega,\kappa}(-L,0)}{1-R^\varepsilon_{\omega,\kappa}(-L,0)}\varepsilon^2\frac{\hat{f}_z(\omega)}{\sqrt{\zeta_0(\kappa)}}e^{-i\frac{\omega}{\varepsilon}\boldsymbol{\kappa}\cdot\boldsymbol{x}_s},$$
$$\hat{b}^\varepsilon(\omega,\boldsymbol{\kappa},0^-) = \frac{2}{1-R^\varepsilon_{\omega,\kappa}(-L,0)}\varepsilon^2\frac{\hat{f}_z(\omega)}{\sqrt{\zeta_0(\kappa)}}e^{-i\frac{\omega}{\varepsilon}\boldsymbol{\kappa}\cdot\boldsymbol{x}_s},$$

which in turn gives

$$\hat{a}^\varepsilon(\omega,\boldsymbol{\kappa},0^+) = \hat{b}^\varepsilon(\omega,\boldsymbol{\kappa},0^+) = \frac{1+R^\varepsilon_{\omega,\kappa}(-L,0)}{1-R^\varepsilon_{\omega,\kappa}(-L,0)}\varepsilon^2\frac{\hat{f}_z(\omega)}{\sqrt{\zeta_0(\kappa)}}e^{-i\frac{\omega}{\varepsilon}\boldsymbol{\kappa}\cdot\boldsymbol{x}_s}$$
$$+\varepsilon^2\frac{\boldsymbol{\kappa}\cdot\hat{\boldsymbol{f}}_{\boldsymbol{x}}(\omega)\sqrt{\zeta_0(\kappa)}}{\rho_0}e^{-i\frac{\omega}{\varepsilon}\boldsymbol{\kappa}\cdot\boldsymbol{x}_s}. \tag{A.15}$$

Substituting into

$$\hat{u}^\varepsilon(\omega,\boldsymbol{\kappa},0^+) = \frac{1}{2\sqrt{\zeta_0(\kappa)}}\big[\hat{a}^\varepsilon(\omega,\boldsymbol{\kappa},0^+)+\hat{b}^\varepsilon(\omega,\boldsymbol{\kappa},0^+)\big]$$

gives (2.26).

A.3. Conservation of Energy Relation. An important relation is the conservation of energy relation. Since $M^\varepsilon_{22} = \overline{M^\varepsilon_{11}}$ and $M^\varepsilon_{12} = \overline{M^\varepsilon_{21}}$, the entries of the propagator matrix satisfy $P^\varepsilon_{22} = \overline{P^\varepsilon_{11}}$ and $P^\varepsilon_{12} = \overline{P^\varepsilon_{21}}$. Moreover, since $\mathbf{M}^\varepsilon$ has trace zero we have $\partial_z\big(\det\mathbf{P}^\varepsilon\big) = \big(\operatorname{Tr}\mathbf{M}^\varepsilon\big)\big(\det\mathbf{P}^\varepsilon\big) = 0$, and therefore $\det\mathbf{P}^\varepsilon = 1$. This gives the conservation of energy relation

$$|R^\varepsilon_{\omega,\kappa}(-L,0)|^2 + |T^\varepsilon_{\omega,\kappa}(-L,0)|^2 = \frac{|P^\varepsilon_{12}(-L,0)|^2+1}{|P^\varepsilon_{22}(-L,0)|^2}$$
$$= \frac{P^\varepsilon_{12}P^\varepsilon_{21}(-L,0)+P^\varepsilon_{11}P^\varepsilon_{22}(-L,0)-P^\varepsilon_{12}P^\varepsilon_{21}(-L,0)}{P^\varepsilon_{11}P^\varepsilon_{22}(-L,0)}$$
$$= 1. \tag{A.16}$$

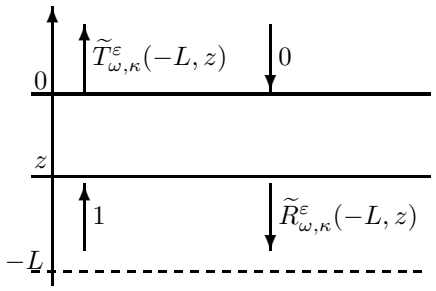

FIG. A.3. *Adjoint reflection and transmission coefficients* $(\widetilde{T}^{\varepsilon}_{\omega,\kappa}, \widetilde{R}^{\varepsilon}_{\omega,\kappa})$.

A.4. Derivation of (2.42-2.44). We consider the situation with an incoming up-going wave coming from the lower half-space:

$$\hat{a}^{\varepsilon}(\omega, \boldsymbol{\kappa}, -L) = \hat{S}^{\varepsilon}_{a}(\omega, \boldsymbol{\kappa}). \tag{A.17}$$

Here there is no other source.

We introduce the adjoint transmission and reflection coefficients $(\widetilde{T}^{\varepsilon}_{\omega,\kappa}, \widetilde{R}^{\varepsilon}_{\omega,\kappa})$ defined by the relation

$$\mathbf{P}^{\varepsilon}(\omega, \kappa, z, 0) \begin{bmatrix} 1 \\ \widetilde{R}^{\varepsilon}_{\omega,\kappa}(z,0) \end{bmatrix} = \begin{bmatrix} \widetilde{T}^{\varepsilon}_{\omega,\kappa}(z,0) \\ 0 \end{bmatrix}, \tag{A.18}$$

which corresponds to the scattering problem for a unit-power incident plane wave incoming from the half-space $(-\infty, z)$ and probing the inhomogeneous layer in $(z, 0)$ with transparent boundary conditions (see Figure A.3). By inverting this matrix-vector relation for $z = -L$ we get

$$\widetilde{T}^{\varepsilon}_{\omega,\kappa}(-L,0) = \frac{1}{P^{\varepsilon}_{22}(\omega,\kappa,-L,0)} = T^{\varepsilon}_{\omega,\kappa}(-L,0), \qquad \widetilde{R}^{\varepsilon}_{\omega,\kappa}(-L,0) = -\frac{P^{\varepsilon}_{21}(\omega,\kappa,-L,0)}{P^{\varepsilon}_{22}(\omega,\kappa,-L,0)}. \tag{A.19}$$

From the relation (A.10) evaluated at $z = 0^{-}$ and $z_0 = -L$, we get using (A.8) and (A.17):

$$\begin{aligned} \hat{a}^{\varepsilon}(\omega, \boldsymbol{\kappa}, 0) &= \frac{P^{\varepsilon}_{11}P^{\varepsilon}_{22}(\omega,\kappa,-L,0) - P^{\varepsilon}_{12}P^{\varepsilon}_{21}(\omega,\kappa,-L,0)}{P^{\varepsilon}_{22}(\omega,\kappa,-L,0) - P^{\varepsilon}_{12}(\omega,\kappa,-L,0)} \hat{a}^{\varepsilon}(\omega, \boldsymbol{\kappa}, -L) \\ &= \frac{\big(\det \mathbf{P}^{\varepsilon}(\omega,\kappa,-L,0)\big) T^{\varepsilon}_{\omega,\kappa}(-L,0)}{1 - R^{\varepsilon}_{\omega,\kappa}(-L,0)} \hat{a}^{\varepsilon}(\omega, \boldsymbol{\kappa}, -L). \end{aligned}$$

Using the fact that $\det \mathbf{P}^{\varepsilon} = 1$ we can simplify the previous expression:

$$\hat{a}^{\varepsilon}(\omega, \boldsymbol{\kappa}, 0) = \frac{T^{\varepsilon}_{\omega,\kappa}(-L,0)}{1 - R^{\varepsilon}_{\omega,\kappa}(-L,0)} \hat{a}^{\varepsilon}(\omega, \boldsymbol{\kappa}, -L).$$

Moreover:

$$\begin{aligned} \hat{b}^{\varepsilon}(\omega, \boldsymbol{\kappa}, -L) &= \frac{1}{P^{\varepsilon}_{22}(\omega,\kappa,-L,0)} \big[\hat{a}^{\varepsilon}(\omega, \boldsymbol{\kappa}, 0) - P^{\varepsilon}_{12}(\omega,\kappa,-L,0)\hat{a}^{\varepsilon}(\omega, \boldsymbol{\kappa}, -L)\big] \\ &= \Big[\frac{(T^{\varepsilon}_{\omega,\kappa}(-L,0))^2}{1 - R^{\varepsilon}_{\omega,\kappa}(-L,0)} + \widetilde{R}^{\varepsilon}_{\omega,\kappa}(-L,0)\Big] \hat{a}^{\varepsilon}(\omega, \boldsymbol{\kappa}, -L). \end{aligned} \tag{A.20}$$

From (A.3-A.4) we obtain

$$\hat{p}^\varepsilon(\omega,\boldsymbol{\kappa},-L)=\frac{\sqrt{\zeta_0(\kappa)}}{2}\Big[\hat{a}^\varepsilon(\omega,\boldsymbol{\kappa},-L)e^{-i\frac{\omega}{\varepsilon}\frac{L}{c_0(\kappa)}}-\hat{b}^\varepsilon(\omega,\boldsymbol{\kappa},-L)e^{i\frac{\omega}{\varepsilon}\frac{L}{c_0(\kappa)}}\Big].$$

Substituting (A.20) and (A.17) into this equation gives (2.42-2.44).

Appendix B. Migration of the Array Response Matrix in a Homogeneous Medium. In this appendix we address the ideal situation in which:
1) the background medium is homogeneous with speed of propagation c_0 and there is a small reflector embedded in this medium at $\vec{\boldsymbol{y}}=(\boldsymbol{y},-L_y)$,
2) the response matrix of the array $(\vec{\boldsymbol{x}}_q)_{q=1}^{N_{\rm q}}$ is available. This means that we have performed a sequence of $N_{\rm q}$ experiments. In the qth experiment a short pulse is emitted from $\vec{\boldsymbol{x}}_q=(\boldsymbol{x}_q,-L)$ (modeled by a source term of the form $f(t)$ in the scalar wave equation) and the signals $p(t,\vec{\boldsymbol{x}}_{q'};\vec{\boldsymbol{x}}_q)$ are recorded by all sensors $\vec{\boldsymbol{x}}_{q'}$ of the array, $q'=1,\dots,N_{\rm q}$.

The Kirchhoff migration function of the array response matrix for the search point $\vec{\boldsymbol{y}}^S$ is:

$$\mathcal{I}_{\rm KM}(\vec{\boldsymbol{y}}^S)=\frac{1}{N_{\rm q}^2}\sum_{q,q'=1}^{N_{\rm q}}p\Big(\frac{|\vec{\boldsymbol{x}}_q-\vec{\boldsymbol{y}}^S|+|\vec{\boldsymbol{x}}_{q'}-\vec{\boldsymbol{y}}^S|}{c_0},\vec{\boldsymbol{x}}_{q'};\vec{\boldsymbol{x}}_q\Big).\tag{B.1}$$

This function produces a good image of the reflector as shown by the following proposition.

PROPOSITION B.1. *If the receiver array at depth $-L$ is a dense square array centered at $\boldsymbol{x}_A$ and with sidelength a, then, denoting the search point by $\vec{\boldsymbol{y}}^S=\vec{\boldsymbol{y}}+(\boldsymbol{\xi},\eta)$, we have*

$$\begin{aligned}\mathcal{I}_{\rm KM}(\vec{\boldsymbol{y}}^S)=&\frac{\sigma_{\rm ref}}{32\pi^3(L_y-L)^2}{\rm sinc}^2\Big(\frac{\pi a\xi_1}{\lambda_0(L_y-L)}\Big){\rm sinc}^2\Big(\frac{\pi a\xi_2}{\lambda_0(L_y-L)}\Big)\\&\times\int\omega^2\hat{f}_z(\omega)\exp\Big(2i\frac{\omega}{c_0}(\eta+\boldsymbol{\xi}\cdot\frac{\boldsymbol{x}_A-\boldsymbol{y}}{L_y-L})\Big)d\omega.\end{aligned}\tag{B.2}$$

Here $\sigma_{\rm ref}$ is the scattering cross section of the reflector and we have simplified the expression by assuming Hypothesis (2.12).

Proof. Using the Born approximation for the reflector, the recorded field is of the form

$$\hat{p}(\omega,\vec{\boldsymbol{x}}_{q'};\vec{\boldsymbol{x}}_q)=\hat{G}(\omega,\vec{\boldsymbol{x}}_q,\vec{\boldsymbol{x}}_{q'})+\sigma_{\rm ref}\omega^2\hat{G}(\omega,\vec{\boldsymbol{x}}_q,\vec{\boldsymbol{y}})\hat{G}(\omega,\vec{\boldsymbol{y}},\vec{\boldsymbol{x}}_{q'}),$$

in the Fourier domain, where $\hat{G}$ is the time-harmonic Green's function of the homogeneous background:

$$\hat{G}(\omega,\vec{\boldsymbol{x}},\vec{\boldsymbol{x}}')=\frac{1}{4\pi|\vec{\boldsymbol{x}}-\vec{\boldsymbol{x}}'|}\exp\Big(i\frac{\omega}{c_0}|\vec{\boldsymbol{x}}-\vec{\boldsymbol{x}}'|\Big).$$

By the triangular inequality, we have $|\vec{\boldsymbol{x}}_q-\vec{\boldsymbol{y}}^S|+|\vec{\boldsymbol{x}}_{q'}-\vec{\boldsymbol{y}}^S|>|\vec{\boldsymbol{x}}_q-\vec{\boldsymbol{x}}_{q'}|$ and therefore the direct field does not contribute to the migration function, only the scattered field can contribute. Using the fact that the array is dense (i.e. the distance between the sensors is smaller than or equal to half-a-central wavelength), we can we apply a

continuum approximation which gives

$$\mathcal{I}_{\rm KM}(\vec{\boldsymbol{y}}^S) = \frac{\sigma_{\rm ref}}{32\pi^3(L_y-L)^2}\int \omega^2 \hat{f}_z(\omega) \\ \times\Big[\frac{1}{a^2}\int_{\boldsymbol{x}_q-\boldsymbol{x}_A\in[-a/2,a/2]^2} \exp\Big(i\frac{\omega}{c_0}(|\vec{\boldsymbol{x}}_q-\vec{\boldsymbol{y}}|-|\vec{\boldsymbol{x}}_q-\vec{\boldsymbol{y}}^S|)\Big)d\boldsymbol{x}_q\Big]^2 d\omega,$$

where we have also simplified the amplitude term by taking into account that $a \ll L_y - L$. Next we expand the difference

$$|\vec{\boldsymbol{x}}_q-\vec{\boldsymbol{y}}|-|\vec{\boldsymbol{x}}_q-\vec{\boldsymbol{y}}^S| \simeq \eta + \frac{\boldsymbol{\xi}\cdot(\boldsymbol{x}_q-\boldsymbol{y})}{L_y-L},$$

which gives the desired result. □

REFERENCES

[1] M. Asch, W. Kohler, G. Papanicolaou, M. Postel, and B. White, Frequency content of randomly scattered signals, SIAM Review, **33** (1991), pp. 519-626.

[2] M. M. Backus, Water reverberations - their nature and elimination, Geophysics, **24** (1959), pp. 233-261.

[3] A. Bakulin and R. Calvert, The virtual source method: Theory and case study, Geophysics, **71** (2006), pp. SI139-SI150.

[4] B. Biondi, *3D Seismic Imaging*, Society of Exploration Geophysics, Tulsa, 2006.

[5] N. Bleistein, J. K. Cohen, and J. W. Stockwell, *Mathematics of Multidimensional Seismic Imaging, Migration, and Inversion*, Springer, New York, 2001.

[6] L. Borcea, J. Garnier, G. Papanicolaou, and C. Tsogka, Coherent interferometric imaging, time gating, and beamforming, Inverse Problems, **27** (2011), 065008.

[7] L. Borcea, J. Garnier, G. Papanicolaou, and C. Tsogka, Enhanced statistical stability in coherent interferometric imaging, Inverse Problems, **27** (2011), 085004.

[8] L. Borcea, F. Gonzalez del Cueto, G. Papanicolaou, and C. Tsogka, Filtering deterministic layering effects in imaging, SIAM Multiscale Model. Simul., **7** (2009), pp. 1267-1301.

[9] L. Borcea, G. Papanicolaou, and C. Tsogka, Interferometric array imaging in clutter, Inverse Problems, **21** (2005), pp. 1419-1460.

[10] L. Borcea, G. Papanicolaou, and C. Tsogka, Adaptive interferometric imaging in clutter and optimal illumination, Inverse Problems, **22** (2006), pp. 1405-1436.

[11] L. Borcea, G. Papanicolaou, and C. Tsogka, Coherent interferometric imaging in clutter, Geophysics, **71** (2006), pp. SI165-SI175.

[12] L. Borcea, G. Papanicolaou, and C. Tsogka, Coherent interferometry in finely layered random media, SIAM Multiscale Model. Simul., **5** (2006), pp. 62-83.

[13] A. J. Calvert, Ray-tracing based prediction and subtraction of water-layer multiples, Geophysics, **55** (1990), pp. 443-451.

[14] A. Derode, E. Larose, M. Tanter, J. de Rosny, A. Tourin, M. Campillo, and M. Fink, Recovering the Green's function from field-field correlations in an open scattering medium, J. Acoust. Soc. Am., **113** (2003), pp. 2973-2976.

[15] M. de Hoop and K. Sølna, Estimating a Green's function from field-field correlations in a random medium, SIAM J. Appl. Math., **69** (2009), pp. 909-932.

[16] W. Elmore and M. Heald, *Physics of Waves*, Dover, New York, 1969.

[17] J.-P. Fouque, J. Garnier, A. Nachbin, and K. Sølna, Time reversal refocusing for point source in randomly layered media, Wave Motion, **42** (2005), pp. 238-260.

[18] J.-P. Fouque, J. Garnier, G. Papanicolaou, and K. Sølna, *Wave Propagation and Time Reversal in Randomly Layered Media*, Springer, New York, 2007.

[19] J.-P. Fouque, J. Garnier, and K. Sølna, Time reversal super resolution in randomly layered media, Wave Motion, **43** (2006), pp. 646-666.

[20] J. Garnier, Imaging in randomly layered media by cross-correlating noisy signals, SIAM Multiscale Model. Simul., **4** (2005), pp. 610-640.

[21] J. Garnier and G. Papanicolaou, Passive sensor imaging using cross correlations of noisy signals in a scattering medium, SIAM J. Imaging Sci., **2** (2009), pp. 396-437.

[22] J. Garnier and G. Papanicolaou, Resolution analysis for imaging with noise, Inverse Problems, **26** (2010), 074001.

[23] J. Garnier and K. Sølna, Coupled paraxial wave equations in random media in the white-noise regime, Ann. Appl. Probab., **19** (2009), pp. 318-346.
[24] J. Garnier and K. Sølna, Wave transmission through random layering with pressure release boundary conditions, SIAM Multiscale Model. Simul., **8** (2010), pp. 912-943.
[25] J. Garnier and K. Sølna, Cross correlation and deconvolution of noise signals in randomly layered media, SIAM J. Imaging Sci., **3** (2010), pp. 809-834.
[26] J. A. Hudson, The parabolic approximation for wave propagation as guided waves, J. Phys. D: Appl. Phys., **13** (1980), pp. 145-152.
[27] A. Ishimaru, *Wave Propagation and Scattering in Random Media*, IEEE Press, Piscataway, 1997.
[28] E. Jakeman and J. G. McWhirter, Correlation function dependence of the scintillation behind a deep random phase screen, J. Phys. A: Math. Gen., **10** (1977), pp. 1599-1643.
[29] W. Kohler, G. Papanicolaou, and B. White, Reflection of waves generated by a point source over a randomly layered medium, Wave Motion, **13** (1991), pp. 53-87.
[30] W. Kohler, G. Papanicolaou, and B. White, Reflection and transmission of acoustic waves by a locally-layered slab, in: *Diffuse Waves in Complex Media (Les Houches, 1998)*, J.-P. Fouque, ed., NATO Sci. Ser. C Math. Phys. Sci., Vol. 531, Kluwer Acad. Publ., Dordrecht, 1999, pp. 347-382.
[31] K. Mehta, A. Bakulin, J. Sheiman, R. Calvert, and R. Snieder, Improving the virtual source method by wavefield separation, Geophysics, **72** (2007), pp. V79-V86.
[32] P. M. Morse and K. U. Ingard, *Theoretical Acoustics*, McGraw-Hill, New York, 1968.
[33] G. Papanicolaou, L. Ryzhik, and K. Sølna, Statistical stability in time reversal, SIAM J. Appl. Math., **64** (2004), pp. 1133-1155.
[34] G. Papanicolaou, L. Ryzhik, and K. Sølna, Self-averaging from lateral diversity in the Ito-Schrödinger equation, SIAM Multiscale Model. Simul., **6** (2007), pp. 468-492.
[35] G. T. Schuster, *Seismic Interferometry*, Cambridge University Press, Cambridge, 2009.
[36] B. M. Shevtsov, Statistical characteristics for wave packet scattering in a layered randomly inhomogeneous medium above a reflecting surface, Radiofiz., **30** (1987), pp. 1007-1012 (pp. 750-754 in English).
[37] K. Sølna and G. Papanicolaou, Ray theory for a locally layered medium, Waves Random Media, **10** (2000), pp. 155-202.
[38] F. D. Tappert, The Parabolic Approximation Method, in Wave Propagation and Underwater Acoustics, Springer Lecture Notes in Physics **70** (1977), pp. 224-287.
[39] B. J. Uscinski, *The Elements of Wave Propagation in Random Media*, McGraw Hill, New York, 1977.
[40] K. Wapenaar, E. Slob, R. Snieder, and A. Curtis, Tutorial on seismic interferometry: Part 2 - Underlying theory and new advances, Geophysics, **75** (2010), pp. 75A211-75A227.
[41] B. White, P. Sheng, and B. Nair, Localization and backscattering spectrum of seismic waves in stratified lithology, Geophysics, **55** (1990), pp. 1158-1165.